Published in final edited form as:
J Comp Neurol. 2012 March 1; 520(4): 848–873. doi:10.1002/cne.22793.

Development and Distribution of Neuronal Cilia in Mouse Neocortex

Jon I. Arellano[1,*], **Sarah M. Guadiana**[2], **Joshua J. Breunig**[3], **Pasko Rakic**[1], and **Matthew R. Sarkisian**[2,*]

[1]Department of Neurobiology, Yale University School of Medicine, New Haven, Connecticut 06510

[2]Department of Neuroscience, McKnight Brain Institute, University of Florida, Gainesville, Florida 32610-0244

[3]Department of Biomedical Sciences, Regenerative Medicine Institute and Department of Neurosurgery, Maxine Dunitz Neurosurgical Institute, Cedars-Sinai Medical Center, Los Angeles, California 90048

Abstract

Neuronal primary cilia are not generally recognized, but they are considered to extend from most, if not all, neurons in the neocortex. However, when and how cilia develop in neurons are not known. This study used immunohistochemistry for adenylyl cyclase III (ACIII), a marker of primary cilia, and electron microscopic analysis to describe the development and maturation of cilia in mouse neocortical neurons. Our results indicate that ciliogenesis is initiated in late fetal stages after neuroblast migration, when the mother centriole docks with the plasma membrane, becomes a basal body, and grows a cilia bud that we call a *procilium*. This procilium consists of a membranous protrusion extending from the basal body but lacking axonemal structure and remains undifferentiated until development of the axoneme and cilia elongation starts at about postnatal day 4. Neuronal cilia elongation and final cilia length depend on layer position, and the process extends for a long time, lasting 8–12 weeks. We show that, in addition to pyramidal neurons, inhibitory interneurons also grow cilia of comparable length, suggesting that cilia are indeed present in all neocortical neuron subtypes. Furthermore, the study of mice with defective ciliogenesis suggested that failed elongation of cilia is not essential for proper neuronal migration and laminar organization or establishment of neuronal polarity. Thus, the function of this organelle in neocortical neurons remains elusive.

INDEXING TERMS

ciliogenesis; forebrain; axoneme; protracted maturation; centrioles; corticogenesis; pyramidal cell; interneuron

The primary cilium of neurons has been mostly over-looked for the last 50 years. Although its presence was occasionally documented in ultrastructural studies using electron microscopy (EM; Dahl, 1963; LeVay, 1973; White and Rock, 1980), the lack of a specific marker for this organelle and intrinsic difficulties with random sampling for cilia with EM

*CORRESPONDENCE TO: Matthew R. Sarkisian, Department of Neuroscience, McKnight Brain Institute, University of Florida, Gainesville, FL 32610-0244, matt.sarkisian@mbi.ufl.edu; Jon I. Arellano, Department of Neurobiology, Yale University School of Medicine, New Haven, Connecticut, 06510, jon.arellano@yale.edu.

did not allow for more extensive studies on their morphology or distribution. More recently, cilia were shown to be enriched with type III adenylyl cyclase (ACIII), a mediator of cAMP signalling typically associated with G-protein-coupled membrane receptors (Bishop et al., 2007). The development of antibodies against ACIII has allowed description of the ubiquitous presence of cilia in neurons in different regions of the brain (Bishop et al., 2007), although confirmation of their presence in specific neuronal cell types is lacking. In addition, little is known about their development and function (for review see Fuchs and Schwark, 2004; Green and Mykytyn, 2010; Whitfield, 2004).

During embryonic development, primary cilia extend from interphase radial glial cells into the lateral ventricles (Cohen et al., 1988; Dubreuil et al., 2007; Li et al., 2011). Loss or reduction in the expression of genes that are important for cilia growth and function (e.g., Ift88, stumpy, and Bardet-Biedl syndrome proteins [BBS]) can lead to cortical morphogenesis defects in mice and human (Bennouna-Greene et al., 2011; Breunig et al., 2008; Rooryck et al., 2007; Willaredt et al., 2008). In the postnatal brain, primary cilia are also found on astrocyte-like neural precursors in the hippocampus that express sonic hedgehog (Shh) signalling machinery and respond to secreted Shh to regulate neurogenesis and differentiation (Breunig et al., 2008; Han et al., 2008).

In addition to ACIII, a few neuronal cilia-specific receptors have been identified, including somatostatin receptor subtype 3 (SSTR3), melanin-concentrating hormone receptor 1 (MchR1), dopamine receptor 1 (D1), and serotonin receptor subtype 6 (5-hydroxytryptamine, 5-HT_6; Berbari et al., 2008; Brailov et al., 2000; Domire et al., 2010; Domire and Mykytyn, 2009; Handel et al., 1999). SSTR3 receptors localize on neuronal cilia in the neocortex, hippocampal CA fields, olfactory bulb, and dentate gyrus neuronal populations (Berbari et al., 2008; Handel et al., 1999). In the hippocampus, SSTR3 appears between postnatal days (P) 0 and 3 in rat (Stanic et al., 2009); however, the neocortical developmental appearance of SSTR3 and other neuronal cilia receptor subtypes is unclear. Recent studies have shown that disruption of these molecules or impairment of ciliogenesis in general can lead to abnormalities in object recognition memory and synaptic plasticity and to obesity (Amador-Arjona et al., 2011; Davenport et al., 2007; Einstein et al., 2010; Wang et al., 2009).

Cilia are composed of a microtubular backbone (the axoneme) surrounded by a specialized membrane that is continuous with the plasma membrane. The axoneme extends from the basal body, a structure derived from the mother centriole (the older of the two centrioles), which can form the cilium in two different ways. In one case, a vesicle from the Golgi apparatus attaches to the mother centriole. The centriole starts growing the cilium inside the vesicle, which eventually fuses with the cell membrane, and the cilium continues growing into the extracellular space. Alternatively, the mother centriole can migrate and anchor to the cell membrane to form the basal body from which the cilium grows into the extracellular space (Sorokin, 1962, 1968; for review see Nigg and Raff, 2009; Pedersen et al., 2008). The process of cilia growth can be rapid upon serum starvation (Ou et al., 2009), whereby the axoneme can quickly disassemble if cells re-enter the cell cycle and subsequently reassemble upon reaching G1/G0 (Tucker et al., 1979a,b).

To our knowledge, there are no studies on the development of cortical neuronal cilia, although it has been shown that failure of neuroblasts to segregate centrioles properly during neurogenesis can result in cortical neurons with multiple centrioles and cilia (Anastas et al., 2011). During neuronal migration, the centrioles are a core component of the centrosome, which aids in guiding neuronal migration (Higginbotham and Gleeson, 2007). Therefore, it would be expected that axoneme extension would occur after cells have completed migration.

This study was designed to address these questions, characterizing the development of cilia in neocortical neurons and their presence in specific neuronal types and describing their morphological features by using different techniques such as Western blot, immunohistochemistry, and ultrastructural analysis.

MATERIALS AND METHODS

Mice

Mice of the CD1 strain (two to four animals per age) were collected on embryonic (E) days (E) 11.5, 13.5, 16, 18.5 and P0, P1, P3, P4, P7, P8, P14, P21, P60, P90, P170, and P365. P0 and older mice were intracardially perfused with saline followed by 4% paraformaldehyde (PFA) in 0.1 M phosphate buffer (PB; pH 7.3). After dissection and fixation, brains were either sectioned (60 μm coronal) in a vibratome or cryoprotected, frozen over liquid N_2, and sectioned (20, 50 or 60 μm coronal) on a cryostat. *Stumpy* mutant brain tissue was generated as previously described (Town et al., 2008). Briefly, a floxed *stumpy* allele was deleted in the presence of Cre under the control of the Nestin promoter. Floxed *stumpy* mice were originally generated on a B6/129 background and then back-crossed onto a B6 background for 10 generations. Floxed mice were then crossed with nestin-Cre deleter mice on a pure B6 background (The Jackson Laboratory). Animal care procedures were performed in accordance with the Laboratory Animal Welfare Act, the *Guidelines for the care and use of laboratory animals* (National Institutes of Health), and the approval of both the University of Florida and the Yale University Institutional Animal Care and Use Committee.

In utero electroporation

We used in utero electroporation to deliver plasmid DNA, pCAGGS-GFP, into fetal cerebral cortices as previously described (Rasin et al., 2007; Sarkisian et al., 2006). Briefly, at E13.5, female CD1 mice were anesthetized by an intraperitoneal injection of ketamine (100 mg/kg) and xylazine (10 mg/kg) diluted in sterile saline. The uterine horns were exposed, and ~1 μl of DNA (0.5 μg/μl) mixed with 0.025% fast green) was microinjected through the uterine wall into the lateral ventricles of the cerebral cortices of the mouse embryos using pulled glass capillaries. Electroporation was achieved by discharging 40 V across the cortex in five 50-msec pulse series spaced 950 msec apart with a BTX ECM 830 Square Wave Electroporator. Following injections, the dams were sutured and allowed to recover on heating pads. Electroporated embryos were harvested at E16.5, and brains were dissected and processed for immuno-EM as described below.

Immunohistochemistry

Tissue sections were probed 24–48 hours at 4°C using the following primary antibodies (dilutions listed in Table 1): rabbit antiadenylyl cyclase (ACIII), mouse anti-NeuN, mouse antiparvalbumin, goat anti-Foxp2, rabbit anti-CDP (aka Cux1), rabbit antipericentrin, mouse monoclonal anticalretinin, mouse antipericentrin, and chicken antigreen fluorescent protein (GFP). After the sections were rinsed in phosphate-buffered saline (PBS; pH 7.2), appropriate species-specific, fluorescent-conjugated secondary antibodies were used (1:200; Jackson Immunoresearch, West Grove, PA) for each antibody. After a rinse in PBS, immunostained sections were coverslipped using ProLong Gold Antifade media containing 4′,6-diamidino-2-phenylindole dihydrochloride (DAPI; Invitrogen, Carlsbad, CA).

For combination of ACIII and pericentrin rabbit antibodies, tissue was incubated first in ACIII and developed with fluorescein isothiocyanate (FITC)-conjugated monovalent Fab secondary antibodies (1:200; Jackson Immunoresearch), followed by incubation in

pericentrin and development in conventional Cy3-conjugated secondary antibodies. No overlapping domains were observed in the cortex, as shown below in Figure 1A.

Antibody characterization

The antibodies used in this study were tested by immunostaining of mouse brain sections or by Western blot analyses of mouse brain lysates. The data that we collected for each antibody were consistent with known information about each protein. Antibody information is detailed in Table 1, with further specificity details listed below.

- Rabbit anti-ACIII was raised against the C-terminal 20 amino acids of mouse ACIII. By Western blot, this antibody can detect bands between ~125 and ~200 kDa depending on the level of glycosylation (Murthy and Makhlouf, 1997; Wei et al., 1996, 1998; Wong et al., 2000). Immunostaining in the brain reveals specific enrichment in neuronal cilia, which was confirmed by the absence of ACIII detection in cilia from ACIII knockout mice (Bishop et al., 2007; Wang et al., 2009). The pattern of staining in our study is consistent with that in the citations given above.
- Mouse monoclonal antibody against β-actin was raised against a modified β-cytoplasmic actin N-terminal peptide (Ac-Asp-Asp-Asp-Ile-Ala-Ala-Leu-Val-Ile-Asp-Asn-Gly-Ser-Gly-Lys) conjugated to KLH. By Western blot, the antibody detects a 42-kDa band (predicted MW of β-actin) from lysates of cultured mouse, human, or chicken fibroblast extracts. Results described below reveal an identical pattern and molecular weight for β-actin (see Fig. 1).
- Mouse monoclonal antibody against calbindin D-28K was produced by hybridization of mouse myeloma cells with spleen cells isolated from mice immunized with calbindin D-28k purified from chicken gut. This antibody specifically stains the ^{45}Ca-binding domain of calbindin D-28k (MW 28 kDa, IEP 4.8) in a two-dimensional gel. By radioimmunoassay, it detects calbindin D-28k with a sensitivity of 10 ng/assay and an affinity of 1.6×10^{12} L/M. Immunoblots of tissue originating from several species including rodents and primates show a band of 28 kDa, and the antibody does not cross-react with other known calcium-binding proteins (Celio et al., 1990). Antibody CB300 immunolabels a subpopulation of neurons in the normal brain with high efficiency but does not stain in the brain of calbindin D-28k knockout mice (Airaksinen et al., 1997).
- Mouse anticalretinin was produced in mice by immunization with recombinant human calretinin-22k (Zimmermann and Schwaller, 2002), an alternative splice product of the calretinin gene and identical to calretinin up to Arg178. The antibody 6B3 stains a 29-kD band (calretinin MW = 29 kD) on immunoblots of brain extracts from mouse, rat, and macaque. Immunohistochemistry with the antibody stains a subpopulation of nonpyramidal cells in the cortex of mice that is absent in CR-KO mice (Bearzatto et al., 2006). The antibody does not cross-react with calbindin D-28K or other calcium-binding proteins as shown by immunoblots or immunostaining in brain tissue.
- Chicken anti-GFP antibody was raised against the recombinant full-length synthetic peptide of jellyfish *Aequorea victoria*. By Western blot analysis of transgenic mouse spinal cord or mouse carcinoma cell lines expressing GFP, this antibody recognizes a distinct band between 27 and 30 kDa (predicted MW of GFP = 27kDa). Immunostaining of untreated wild-type brain tissue with this antibody showed no detectable staining.

- Mouse monoclonal against neuron-specific nuclear antigen (NeuN) was originally made against cell nuclei purified from mouse brain, and Western blotting with this antibody shows three bands in the 46–48-kDa range (Mullen et al., 1992). The anti-NeuN antibody showed a pattern of neuronal nuclei in the developing mouse brain like that previously described (Mullen et al., 1992). We also observed NeuN in the neuronal cell body, which is consistent not only with previous reports (Kao et al., 2008; Lyck et al., 2007; Saino-Saito et al., 2011) but also with recent identification of NeuN as splicing regulator Fox-3, which appears to have isoforms that localize to the cytoplasm (Dredge and Jensen, 2011; Kim et al., 2009).
- Mouse monoclonal antiparvalbumin reacts specifically with parvalbumin (PV) in cultured nerve cells and in mouse tissue and specifically stains the ^{45}Ca-binding spot of PV (MW = 12 kDa and IEF 4.9) in a two-dimensional “immunoblot.” (Celio and Heizmann, 1981). Staining was located in a subpopulation of nonpyramidal cells in the neocortex as previously described (Cho et al., 2011).
- Rabbit polyclonal antibody anti-pericentrin was raised against a fusion protein containing 60 kDa of pericentrin (amino acids 870–1370 of the mouse protein) and T7-gene10 (Doxsey et al., 1994). This antibody recognizes a single 220-kDa band by immunoblotting and has been extensively characterized in a previous study (Doxsey et al., 1994). Staining in the developing neocortex showed a pattern of pericentrin immunoreactivity that was identical to previous descriptions (Westra et al., 2008).
- Mouse monoclonal anti-pericentrin was raised against amino acids 1692–1814 of mouse pericentrin and purified by affinity chromatography. As described in an original characterization of pericentrin (Doxsey et al., 1994), this antibody detects a band at 220 kDa (MW of pericentrin). The pattern of immunostaining with this antibody is also comparable to other studies showing enrichment in centrioles (Jurczyk et al., 2010) and is also similar to the rabbit pericentrin, with which we found to be localized to the basal body at the cilium base.
- Rabbit polyclonal anti-Cux1 (anti-CDP) was raised against amino acids 1111–1332 of CDP (CCAAT displacement protein) of mouse origin. On Western blot of mouse liver extracts, this antibody detects a band at ~200 kDa, which is knocked down by specific micro-RNAs (Xu et al., 2010). This antibody has also been shown by multiple investigators to label neurons effectively in upper layers 2/3 of neocortex (Feng and Cooper, 2009; Tury et al., 2011). The pattern of staining in our study is consistent with these earlier studies.
- Goat anti-Foxp2 was raised against a synthetic peptide REIEEEPLSEDLE corresponding to C-terminal amino acids 703–715 of human FOXP2 protein. On Western blot analysis of human cerebellum lysates, this antibody detected a single band at ~ 80kDa (predicted MW = ~79.9 kDa; manufacturer’s technical information). Staining for Foxp2 reveals strong expression in neuronal nuclei of deep layers of neocortex (Ferland et al., 2003; Stillman et al., 2009; Waclaw et al., 2010). The patterns of antibody staining in our study resemble those reported in the studies cited above.

Analysis and quantification of cilia

For quantification of cilia length, mice at P0, P4, P7, P14, P60, P90, P170, and P365 were analyzed (two brains/age and two sections/brain) in area S1Tr from the mouse brain atlas (Paxinos and Franklin, 2004), located dorsal to the hippocampus and medial to the barrel field cortex. Vibratome sections (60 μm) were immunostained for ACIII and NeuN and counterstained with DAPI. Mosaic stacks (9–18 images separated ~1 μm in the z axis) were

taken from the pial surface to the white matter using a Zeiss Apotome system attached to a Zeiss Axioplan2 microscope with a ×20 objective using Zeiss Axiovision software. Stacks were collapsed to the maximum intensity projection, and the resulting images were adjusted for gray levels for each channel using the same software. Images were imported into Reconstruct software (Fiala, 2005), where they were aligned, layers were delimitated, and cilia were traced and measured. In total 3,756 cilia were measured, averaging ~85 per layer and age studied, in this analysis performed by J.I.A. In addition, a separate analysis was performed by S.M.G. at ages E18.5, P0, P3, P7, P14, P21, P60, P90 using an Olympus IX81-DSU spinning disc confocal microscope. Z-stacks of images (at 0.75 μm steps) of sections immunostained for ACIII (Santa Cruz Biotechnolgy, Santa Cruz, CA) and pericentrin (BD Biosciences, San Jose, CA) were collected and subsequently collapsed to the maximum intensity projection. Resulting images were analyzed in Image J64 (http://rsbweb.nih.gov/ij/), in which cilia lengths were measured from the pericentrin puncta side to the end of the continuous $ACIII^+$ signal in at least two brains and six to eight fields/section for each age. Although not displayed, similar results were obtained in both analyses. For analysis of $ACIII^+$ cilia extending from PV^+ cells, Z-stack images of sections immunostained for ACIII and PV were converted to maximum intensity projection images, and $ACIII^+$ cilia lengths were analyzed in Image J64 as described above. Analyses of cilia length between sexes were compared by Student's *t*-tests (two tailed). In all tests, $P < 0.05$ was considered significant.

Electron microscopy

For the immuno-EM analysis, electroporated brains were fixed at E16.5 by immersion in 4% PFA and 0.3% glutaraldehyde in PB for 24 hours at 4°C. Brains were dissected, embedded in 4% agarose, and sectioned (100 μm thick) with a vibratome (Leica). Sections were collected in PB, cryoprotected with 30% sucrose, and freeze-thawed over liquid nitrogen to permeabilize the tissue. After being rinsed in PB, sections were incubated with antibodies against GFP for 24 hours, rinsed in PB, incubated with biotinylated secondaries (Jackson Immunoresearch) for 2 hours, rinsed in PB, incubated in an ABC Elite kit (Vector, Burlingame, CA), rinsed in PB, and developed with diaminobenzidine (DAB; Vector) as chromogen. From this point, sections were postfixed and processed for EM in the same way as described below.

For the conventional EM analysis, animals were intracardially perfused with saline followed by 4% PFA in PB for P60 brains and 1% PFA and 1.25% glutaraldehyde in PB for the rest of the ages. Brains were dissected and postfixed in the same fixative overnight. After being rinsed in PB, brains were sectioned (60–100 μm thick) coronally with a vibratome. Animals P8 or younger were embedded in 4% agarose before sectioning. P60 sections were collected in PB and postfixed in 2% glutaraldehyde for 1 hour. All sections were postfixed in 1% osmium tetroxide for 40 minutes and then rinsed, dehydrated, embedded in Durcupan (Fluka, Buchs, Switzerland), and cured in an oven for 48 hours at 60°C. Neocortical regions of interest were sectioned at 70 nm in a Reichert ultracut ultramicrotome. Serial sections were collected in slot grids covered with Formvar, counterstained with uranyl acetate and lead citrate, and analyzed in a Jeol JEM-1010. Pictures were taken with a Gatan MSC600W digital camera and adjusted for brightness and contrast in Adobe Photoshop.

Western blots

Protein lysates from mouse cortex were prepared by homogenizing tissue in 1× RIPA buffer (containing 20 mM Tris-HCl, pH 7.5, 150 mM NaCl, 1 mM Na_2EDTA, 1 mM EGTA, 1% vol/vol Triton X-100, 2.5 mM sodium pyrophosphate, 1 mM glycerophosphate, 1 mM Na_3VO_4, 1 mg/ml leupeptin, and 1 mM PMSF; Cell Signaling, Beverly, MA). For developmental time points, similar total amounts (30 μg/lane) were loaded onto 4–12%

NuPAGE gel (Invitrogen) and separated by SDS-PAGE. Proteins were transferred onto PVDF membranes using an iBlot (Invitrogen). Blots were blocked in 5% BSA in Tris-buffered saline containing 0.1% Tween (TBST) for 1 hour at RT. The following primary antibodies were diluted in 2.5% BSA in TBST incubated overnight at 4°C: rabbit anti-ACIII or mouse anti-β-actin. Membranes were rinsed in TBST, and incubated with appropriate horseradish peroxidase (HRP)-conjugated secondary antibodies (1;10,000; Bio-Rad, Hercules, CA). Blots were developed using chemiluminescence (ECL-Plus Kit; GE Healthcare, Picataway, NJ), and images were captured with an Alpha Innotech FluorChemQ Imaging System (Cell Biosciences).

RESULTS

Expression of ACIII in fetal and postnatal mouse cortex

Cilia throughout the mature cortex are enriched in ACIII (Bishop et al., 2007), which thus serves as a surrogate cilial marker (Fig. 1A). To study the expression of ACIII in the developing cortex, we used Western blot analysis to examine protein lysates from mouse cortex at ages E11.5, E13.5, E16, E18.5, P0, P7, P14, P21 and young adult (P60; Fig. 1B). We found low levels of ACIII at ~E13.5 (roughly midcortical neurogenesis), but levels were higher at birth and noticeably increased over the first few postnatal weeks (Fig. 1B). ACIII persisted at P60, but the signal intensity was lower compared with P21 lysates (Fig. 1B). Quantification of ACIII relative to β-actin from the same blot confirmed these observations (data not shown). We found that the signal for ACIII is ~125–130 kDa, suggesting that cortical ACIII might be predominantly in a less glycosylated form (Murthy and Makhlouf, 1997; Wei et al., 1996). To confirm this, we compared lysates isolated from P90 olfactory epithelium and frontal cortex from the same brain. As reported previously (Wong et al., 2000), we observed a very strong signal for glycosylated ACIII between ~190 and ~200 kDa in olfactory epithelium, which was not observed in cortex (Fig. 1C). Taken together, these data suggest that ACIII, a protein enriched in neuronal cilia, is expressed mostly in a less glycosylated form in the neocortex, which increases in the late embryonic stages, becoming more robust in postnatal cortex.

Basal body docking begins in deeper layer cells of the developing cortical plate

To study the possibility of late embryonic growth of neuronal cilia, we analyzed sections of mouse cortex that had been electroporated at embryonic day (E) 13.5 with a plasmid expressing GFP and subsequently fixed at E16.5 and prepared for immuno-EM. We first screened cells localized throughout the cortical plate (CP; Fig. 2A,B) for the presence and location of cilia and centrioles/basal bodies (quantified in Fig. 2C). We found only a few cilia precursors at a very early stage of development (Figs. 2D–F, 3), and most cells exhibited centrioles either free in the cytoplasm (undocked centrioles; Figs. 2G–I, 3A) or located adjacent to the cell membrane with one centriole attached to the plasma membrane (docked centrioles/basal bodies; Figs. 2D–F, 3B,C). The centrioles appeared surrounded by or in close proximity to Golgi apparatus, and in some cases multivesicular bodies were also observed in their vicinity (Fig. 3A,C).

Results of our analysis are summarized in Figure 2C. From among 36 centriole encounters in the deeper CP, 25 were docked with the membrane, whereas 11 were undocked (Fig. 2C). Electroporation of a cohort of neural progenitors from the ventricular zone with GFP cDNA allowed us to track the neural cells derived from them. Cells generated at E13.5 and later are directed mostly to upper layers of the neocortex, so GFP^+ cells located in the deep CP at E16.5 would most likely be migrating cells. In fact, docked centrioles were frequently within non-GFP^+ cells that typically displayed ultrastructural features of nonmigrating cells (e.g., more rounded soma, less elongated nuclei) both in the upper and in the deep CP (e.g.,

Fig. 2D–F). In contrast, undocked centrioles in the deeper CP were in GFP^+ cells that also typically exhibited leading processes and elongated nuclear morphology, suggesting that they were in fact cells migrating to upper layers (e.g., Fig. 2G). Moreover, deep CP cells with docked centrioles sometimes exhibited short (0.1–0.5 μm) protrusions consisting of a membranous bud lacking microtubular organization that we called procilia (e.g., Figs. 2E,F, 3). We found only rare cases of undocked centrioles with a vesicle attached (Figs. 2G, 3A) that could represent the previous step before docking of the centriole to the cell membrane (Pedersen et al., 2008). The relative rarity of these findings suggests that vesicle attachment to the mother centriole could be quickly followed by centriole docking to the cell membrane. According to this model, ciliation of immature neurons would occur at the cell membrane and not inside the vesicle attached to the mother centriole.

In upper CP, 27 of 31 centrioles were undocked (Fig. 2C,H,I). Thus ~70% of deeper layer cells possess a docked centriole, whereas only ~10% of upper CP cells contained similarly docked centrioles. These data suggest that cells initiate docking of the mother centriole in the CP once cells have completed migration and/or reached their appropriate lamina.

Neuronal primary cilia axonemes develop postnatally taking several weeks to reach maximal lengths

In the rodent cortex, the cilia and basal bodies are immunodetectable with ACIII and pericentrin, respectively (Anastas et al., 2011; Bishop et al., 2007; Wang et al., 2011; Fig. 4A–E). To study the development of neocortical cilia, ACIII immunostaining and EM were used at different ages. Cilia length was estimated by tracing ACIII signal on collapsed confocal z-stack images from tissue sections at P0, P4, P7, P14, P60, P90, P170, and P365. Average and maximum cilia lengths were recorded for each age and cortical layer (Table 2, Fig. 4F). ACIII staining revealed regional and laminar differences in the length of cilia in the neocortex. To avoid regional bias, we consistently measured cilia in the dorsal neocortex overlying the hippocampus (for details see Materials and Methods). To distinguish laminar differences, we used DAPI and NeuN to delineate layers 1–6 when possible (Fig. 5). These methods do not allow for the establishment of absolute values of cilia length but provide information about cilia elongation trends in different cortical compartments over time. In total 3,756 cilia were measured, averaging ~85 per layer and age studied. To correspond with our analysis of ACIII, EM studies were performed at P0, P4, P8, and P60 to assess structural developmental characteristics.

At E18.5 and P0, ACIII staining revealed a punctate pattern suggesting slightly elongated growth of cilia compared with E16.5 (Figs. 4A,B, 5A–D, Table 2). NeuN is not fully expressed by all neurons in the region analyzed at P0 and is almost absent in layer 2, upper layer 3, and deep layer 6, although many neurons in the subplate are intensely immunostained. Thus, we only made a distinction between superficial (layers 2–4) and deep (layers 5 and 6) strata based on cytoarchitecture and NeuN expression (Fig. 5A–D). ACIII was found in small specks in all layers, with rare rod-like cilia. Layer 1 had short cilia compared with the CP, in which both superficial and deep strata showed similar lengths (Table 2, Figs. 4F, 5A–D). Ultrastructural analysis at P0 supported those findings and showed the presence of procilia in all cells analyzed (n = 21), although with large heterogeneity in their length (Figs. 6, 7). These procilia were similar to some observed at E16.5 (Figs. 2D–I, 3, 6), but they had different ciliar content. Sometimes they exhibited a short axoneme, with doublets of outer microtubules poorly developed and distinguishable only for about 100–200 nm into the procilium. The presence of vesicles was a common finding inside the procilia (see. e.g., Fig. 6B,C), and some procilia appeared to be filled with a number of vesicles of different size (Fig. 7B,C). Interestingly, we found one cell located in the subplate region bearing a short cilium, but with a well-organized axoneme (Fig. 7D).

At P4, NeuN expression is not fully mature and is very weak in layer 2 and deep layer 6 (Fig. 5E,G,J). Layer 1 at P4 showed relatively long cilia compared with upper layers 2–4, where most ACIII staining appeared as thick punctae (0.7–1.5 μm), with few intermingling longer cilia (2–3 μm; Fig. 5F–H). In deeper layers 5 and 6, the heterogeneity was more dramatic, and two clear populations could be distinguished: a majority of short punctae (0.5–2 μm) and a population of longer cilia especially in some cells in layer 5 (up to 6.6 μm) and in the subplate (up to 5.4 μm; Table 2, Figs. 4F,G, 5I–K). These results suggest that most cilia in upper and deep layers remained in a procilia stage, although some specific subpopulations in deeper layers start elongating earlier. Consistently with this, from the EM analysis at P4 in supragranular layers 1–4, we found only procilia in the cells studied (n = 11; Fig. 8). The procilia at P4 were slightly longer but similar to those described for P0. They showed occasional vesicle-like structures and diffuse electron-dense material, and sometimes the membrane was expanded in a mushroom-like shape (Fig. 8A–C). Similar to P0, procilia at P4 had short and poorly organized axonemes, extending about 200 nm into the procilium, and in deeper layer cells microtubules were observed but lacked clear axonemal organization (Fig. 8D–F). From P4 to P7, upper layer cilia showed an increase in length to match deeper layers lengths (Figs. 4F,G, 5, 9), and all layers had similar average cilia length between 3 and 4.4 μm, with maximum lengths of about 7 μm in layers 2, 3, and 5 (Table 2, Figs. 4F,G, 9). From this age onward, ACIII staining of cilia showed an intense pattern in the proximal segment that tapered toward the tip (Figs. 1A, 4C–E). Consistent with immunohistochemistry results, EM analysis at P8 revealed longer, straighter cilia with a developed axoneme that can be followed several micrometers into the parenchyma (Fig. 10). Unfortunately, the lengthening of cilia creates technical difficulties in following the entire cilium length across a series of EM sections. Thus, for this age onward, we do not have information on the structure of the tip of cilia.

At P14 and P60, there is a progressive elongation of cilia in all layers (Table 2, Figs. 4F,G, 9H–N) and ultrastructural analysis at P60 showed well-developed axonemes and rounded cilia that could be only partially reconstructed (Fig. 11). At P90, ACIII staining showed similar or only slightly longer cilia lengths in all layers compared with P60, suggesting that cilia stop growing by ~P60–P90. Cilia exhibited maximum lengths at these ages, with averages of ~5 μm in layers 2–4 and 6, and ~6 μm in layer 5. Maximum values in each layer varied from ~8 μm in layers 2, 4, and 6 to ~9 μm in layer 3 and to 10.8 μm in layer 5 (Table 2, Fig. 4F,G).

We found a notable shortening of the estimated cilia length at P170 and P365 compared with P60–P90 (Table 2, Fig. 4F,G). This could be due to an actual shortening of cilia, although an alternative possibility is that in aging animals ACIII protein does not fill the cilia completely and is absent from the distal tip. In fact, there were also slight decreases in estimated cilia length in layer 1 and 2 between P60 and P90 that could be due to the same phenomenon (see Discussion).

To determine whether sex had any significant influence on cilia length, we examined the average length in upper and deeper layers of the neocortex of males (n = 2) and females (n = 2) at P14. This analysis did not reveal significant differences in cilia length between sexes (3.06 ± 0.19 μm and 3.03 ± 0.19 μm [mean ± SEM] for males and females, respectively [Fig. 4H]). Taken together, our results suggest that cilia elongation in neocortex is a slow process that starts postnatally with slightly different dynamics depending on cortical layer but is not significantly affected by gender. Maximal cilia length is different depending on cortical layer, and overall it can take up to 3 months to be reached.

Extension of cilia from Ca^{2+} binding protein-containing interneurons

Although $ACIII^+$ cilia have been described for cultured hippocampal cells expressing glutamate acid decarboxylase (Berbari et al., 2007), their presence in inhibitory neurons in the neocortex has not been described. Inhibitory neurons migrate tangentially into the neocortex during development to invade the CP (Wonders and Anderson, 2006). Inhibitory interneurons can be identified by the expression of several markers. From those, calcium-binding proteins parvalbumin, calbindin, and calretinin distinguish three large subpopulations of inhibitory interneurons with little overlap (Defelipe et al., 1999). In the mature rodent cortex, parvalbumin-expressing neurons make up ~50% of GABAergic inhibitory interneurons (Wonders and Anderson, 2006). We examined confocal z-stack images of P60 tissue sections immunostained for PV, ACIII, and NeuN and measured cilia from these cells compared with cells that did not express PV (Fig. 12A–G). PV^+ cells appeared to extend a cilium from the soma (Fig. 12A–F). We found that the lengths of cilia from PV^+ neurons appeared comparable to those of neighboring PV^- neurons (putatively excitatory neurons; mean $PV^+ = 5.12 \pm 0.42$ μm SEM; $PV^- = 5.06 \pm 0.25$ μm; Fig. 12G). In addition, $ACIII^+$ cilia were found in other interneuron subtypes expressing calbindin and calretinin (Fig. 12H–R). These results suggest that neocortical interneurons also extend $ACIII^+$ cilia that reach lengths similar to those of neighboring excitatory pyramidal neurons.

Neuronal cilia do not appear critical for neuronal polarity or expression of layer-specific markers

On pyramidal neurons, cilia generally extend from the base of the apical dendrite (Anastas et al., 2011). This suggests that cilia could be related to the orientation/polarity of neocortical neurons and particularly to the extension/orientation of the apical dendrite. To analyze this, we examined neocortical neurons in *Stumpy conditional* mutant (Δ*Stumpy; NestinCre;Stumpy*$^{fl/fl}$) mice in which all neural cell types (including neurons) either lack or extend a poorly formed, stunted cilia (Breunig et al., 2008; Town et al., 2008). Although the lack of cilia leads to hydrocephalus and noticeable compression of the neocortex starting at approximately P4 (Fig. 13), we still observed properly oriented neurons with apical dendrites in Δ*Stumpy* brain (Fig. 13A–C). In addition, laminar-specific marker expression was preserved in Δ*Stumpy* mice (Fig. 13D,E). These data suggest that failure of neurons to extend normal cilia does not dramatically alter polarity or gross laminar pattern of neurons in the neocortex.

DISCUSSION

Previous studies in vitro and in vivo have gone a long way toward characterizing neuronal cilia and the expression of specific proteins within these structures (for review see Green and Mykytyn, 2010; Lee and Gleeson, 2010). Indeed, there is growing evidence that dysgenesis of the primary cilium can be associated with neurological disorders (Sharma et al., 2008). In addition, during the past decade, much has been learned about the cell biology of ciliogenesis (Goetz and Anderson, 2010). However, the genesis of neuronal cilia during brain development has not been well characterized.

Our results suggest that ciliogenesis in mouse cortical neurons initiates after cells complete migration by docking of the mother centriole to the cell membrane and growing a procilium: a rudiment of the cilium lacking axonemal organization that will largely develop and elongate postnatally. The elongation of neocortical cilia is a surprisingly protracted process lasting for several weeks that follows different temporal patterns and reaches different final lengths depending on laminar position. In addition to pyramidal neuron cilia, we describe the presence of cilia in interneurons, with lengths comparable to those in pyramidal cells.

Collectively, our study provides a comprehensive initial characterization of neuronal ciliogenesis and cilia distribution in the developing and mature mouse neocortex.

Initiation of ciliogenesis in the developing CP

EM analysis of the CP at E16.5 showed frequent undocked centrioles in cells with migratory morphology in the upper layer of the CP, whereas cells with a nonmigratory profile in deeper layer showed predominant basal body docking and in some cases budding procilia. These observations suggested that cessation of migration is a necessary step before docking of the mother centriole to the membrane and the subsequent ciliogenesis. Furthermore, because centrioles are an integral part of the centrosome during neuronal migration (Higginbotham and Gleeson, 2007; Tsai et al., 2007), this conclusion is not unexpected. It is also not surprising that the laminar positions of neocortical neurons are not dramatically altered in brains of mice that have mutations in genes that disrupt neuronal ciliogenesis, because the centrioles have already performed their role in migration prior to docking.

Detailed analysis of the centrioles of cortical cells at E16.5 showed the presence of procilia or short membranous protrusions (0.1–0.8 μm long) growing in the distal aspect of the mother centriole. Serial section analysis revealed that these procilia were present in cells with docked centrioles and in some cases also inside a vesicle attached to undocked centrioles, most likely immediately before docking to the membrane (Sorokin, 1962, 1968; for review see Pedersen et al., 2008). We cannot discard the possibility that some form of cilia could be present at earlier stages of development or in other pallial compartments, for example, in early-migrating immature neurons or in the population of immature neurons with multipolar morphology in the intermediate zone. However, if there is any previous form of cilia, it is very likely transient and probably reabsorbed before final migration of the neurons to their destination in the cortex, insofar as our data suggest that cilia are not present in migrating neurons in the CP. More extensive studies are needed to assess this possibility.

From our data we propose the following model (Fig. 14). When a migrating neuron reaches its appropriate lamina, the mother centriole migrates and docks with the nearby plasma membrane, either directly or attaching a vesicle to their distal tip prior to docking (Sorokin, 1968). Membrane docking generally occurs close to the proximal portion of the leading process that will become the apical dendrite (present results; Anastas et al., 2011). Once the mother centriole docks to the membrane, the procilium grows slightly (~0.2–0.5 μm) and reaches about 0.5–2 μm by P0 and P4. We differentiate procilia from cilia based on the lack of axonemal organization. We define the procilia as membranous protrusions characterized by the lack of axoneme that instead have only an axonemal rudiment extending about 100–300 nm into the procilia. The procilia cytoplasm is filled with diffuse material and frequently contains vesicles and rod-like structures and occasionally short and disorganized microtubules. The term *procilia* has been used by other investigators (Morris and Scholey, 1997; Sfakianos et al., 2007) to describe short, budding cilia in different contexts, sometimes including a well-developed axoneme.

Our description of procilia matches previous observations of the budding primary cilia in diverse avian and mammalian tissues (Sorokin, 1962, 1968) and in the chick developing neural tube (Sotelo and Trujillo-Cenoz, 1958). However, Sotelo and Trujillo-Cenoz reported various cycles of complete ciliogenesis in a period of 4.5 days, indicating a quick assembly of cilia (with fully elongated axoneme), in sharp contrast to the very slow development of procilia from E16.5 to P0 and P4 recorded in our study. We cannot entirely rule out the possibility that the developing axoneme in budding cilia of young neurons is susceptible to rapid microtubule breakdown before the specimen is fully fixed, a possibility that would explain the lack of axoneme at early ages. However, this alternative is in doubt given our observations of cilia with wellorganized axonemes in P0 tissues. In fact, it should be

emphasized that cilia development is not a synchronous and homogeneous process in the neocortex and that differences in length and axonemal content are present particularly at early postnatal times. For example, in the same brain in which we detected (rare) neuronal cilia in the deepest CP with well-developed axonemes, we also observed (rare) neurons in the upper CP with docked centrioles lacking a clear procilium. This difference in cilia development would seem to follow the inside-out pattern of corticogenesis and to correlate with the length differences observed with ACIII staining. Furthermore, at P0, ACIII staining revealed occasional neurons in the subplate exhibiting relatively longer procilia than other layers, suggesting that those cells could display more mature axonemes than the ones found at the EM level. Similarly, at P4, ACIII staining revealed some relatively long procilia located in the subplate and in a subpopulation of neurons in layer 5. EM analysis at the same age revealed lack of axonemes in all procilia analyzed, but procilia in neurons in the deep CP were frequently enriched with microtubular content, suggesting the beginning of axonemal development. Based on this, we propose that axoneme elongation begins ~P0 only in some cells in the subplate, but it is an ongoing process that develops further by P4 in the deep CP and extends subsequently to all layers and probably parallels the cilia elongation pattern reported from ACIII staining. In fact, the axoneme was first observed in all layers at P8, coincident with significant ACIII immunodetection by Western blot and growth in length of cilia. This coincidence suggests that axoneme development is probably responsible for the secondary elongation of the cilia.

Although we focused our study on neurons, at P0 and P4 the high packing density of cortical cells and the incomplete expression of NeuN (Lyck et al., 2007) preclude the selective study of neurons. Therefore, it is possible that some $ACIII^+$ particles would belong to non-neuronal cells. With animals older than P4, we could analyze neuronal cilia more reliably because of the lower neuronal density and mature NeuN expression. However, some cilia could be incomplete as a result of section trimming, and we are measuring the planar projection of cilia and therefore underestimating their length. Therefore, our quantification study is not intended to provide precise values for neuronal cilia length but seeks to give a general picture of cilia distribution and elongation in different cortical layers during development. Similarly, we focused on cells with neuronal features in our EM analysis, but we cannot discard the possibility that some nonneuronal cilia were included in the study.

From P7 onward, a more or less steady elongation of cilia is observed, first and faster in deep layers, which is followed later by upper layers. Length values stabilize between P60 and P90, with average lengths of about 5 μm in all layers, except for layer 5, which has longer cilia (~6 μm on average and up to ~11 μm), far from the maxima in other layers. Layer 1 is unlike layers 2–6 because of its scarce neuronal content, but, as expected, the few neurons detectable with NeuN typically exhibited a long cilium enriched with ACIII. Initially, layer 1 neurons displayed long cilia compared with upper laminae, but after P7 their values were similar to those of other layers. These laminar differences in length and rate of growth could be related to differences in neuron/soma size and maturation rate in different layers (Lund et al., 1977; Van Eden and Uylings, 1985), but we did not study those relationships in the present work. On the other hand, we did not find significant differences in estimated cilia length between sexes.

Surprisingly, we found that the lengths of cilia at P170 and P365 were decreased compared with P60–P90. The explanation for this decrease is currently unclear. It is possible that cilia slightly shorten with aging, but another possibility is a reduced or incomplete localization of ACIII in older animals. ACIII staining tapers toward the tip of the cilium (Poole et al., 1997; present results), so reduced levels of ACIII could lead to incomplete filling of the cilia length. Separate studies on aged rats (>3 years) did not show significant cilia shortening

(data not shown), suggesting that cilia, as visualized with ACIII, do not continue to shorten with advanced aging. Further studies are needed to clarify these questions.

Overall, our study shows that ciliogenesis is a protracted process in mouse neocortex: procilia seem to remain undifferentiated from late fetal to early postnatal stages, and the subsequent elongation of axonemes and cilia takes several weeks to complete, until P60–P90 (Fig. 14). This delayed time course of cilia maturation is very surprising given that cilia growth can be very rapid (on the order of hours) in many nonneural cells in culture (Tucker et al., 1979a,b) and on the order of days in the chick neural tube (Sotelo and Trujillo-Cenoz, 1958). Furthermore, cilia are observed within days on cultured neurons (derived from fetal/perinatal tissues) from a variety of brain regions, including hippocampus, striatum, amygdala, cerebellum, and spinal cord (Barzi et al., 2010; Belgacem and Borodinsky, 2011; Berbari et al., 2007; Domire et al., 2010; Miyoshi et al., 2009). It is difficult to compare the growth that we see in vivo with that of these newly maturing neurons until studies are performed that describe the in vivo development of these structures in each brain region. It is noteworthy that neurons from different brain regions grow cilia of different lengths (Fuchs and Schwark, 2004), but determining whether neurons from different brain regions exploit different mechanisms to control the onset and duration of ciliogenesis requires further analysis. With respect to neocortex (and possibly other regions), prolonged maturation of cilia overlaps with neocortical neuron maturation that comprises key developmental processes such as dendrite growth and synaptogenesis, processes that are defined by actin and microtubule rearrangements and extensive vesicle trafficking, similar to ciliogenesis (Kim et al., 2010). Whether the coincidental developmental time frames of cilia and other neuronal processes are interrelated also requires further study.

Appearance of signalling machinery in neuronal cilia

ACIII can exist at different molecular weights (e.g., ~125 and ~200 kDa) based on glycosylation (Wei et al., 1996). We found that ACIII from cortex appeared to be in the less glycosylated ~125 kDa form as reported by others (Murthy and Makhlouf, 1997). We also found that this differed from the more glycosylated form that is observed in lysates of olfactory epithelium (Wong et al., 2000; present study). The significance of these different forms of ACIII between different brain regions is unclear.

Our analysis of ACIII protein in fetal cortical lysates showed early detection at very low levels at E13.5, E16, and E18.5. These results could correspond to the formation of procilia starting at E13.5, although we cannot rule out the possibility that our blots are detecting nonneuronal or potentially nonciliar ACIII expression. At E18.5, we observed short ACIII$^+$ procilia coinciding with pericentrin$^+$ basal bodies. Later, as development continues postnatally, ACIII expression levels increase dramatically, which directly correlated with the elongation of ACIII positive cilia throughout the neocortex. These levels may also correlate with the cellular production or available levels of cytosolic tubulin, which recently were reported to correspond to cilia length (Sharma et al., 2011). It is unclear why the levels of ACIII protein at P60 appear to be lower than earlier in development. Whether this reflects a role for ACIII earlier in development during cilia elongation (Ou et al., 2009), a change in ACIII concentration within cilia over time, or some other mechanism requires further study.

From E16.5 through P0 until ~P4, our EM analysis showed a slight growth of the prociliar length without apparent axonemal development (except for some subplate cells). The elongation of the cilia axoneme is coordinated by intraflagellar transport (IFT), a bidirectional trafficking mechanism to shuttle cilia components to and from the cilium tip (Pedersen and Rosenbaum, 2008). Mutations in IFT molecules are often associated with defective assembly of primary cilia. For example, Pazour and colleagues (2000) showed that impairment of IFT in mice resulted in short cilia resembling the procilia shown here. Thus, it

is tempting to speculate that IFT might not be fully active at these early stages of ciliogenesis, and later development of this mechanism could be responsible for axoneme and cilia elongation. This is one potential hypothesis for future studies on neuronal cilia.

The EM micrographs typically revealed Golgi apparatus and different types of vesicles in close apposition to the basal body and centriole and also inside the procilia, suggesting that trafficking to the newly forming cilium might be significant at these ages. The presence of ACIII in procilia from E18.5 to P4, when the axoneme is poorly developed, suggests that ACIII localization to the procilium is, or at least can be, independent of the presence of a fully developed axoneme. This is notable in light of the fact that downregulation of BBS2 and BBS4 (Bardet-Biedl syndrome proteins, which regulate vesicular transport to the cilium) impedes SSTR3 but not ACIII localization in cilia and does not notably alter cilia elongation (Berbari et al., 2008). For cell lines, it has been suggested that ACIII can contribute to the elongation of cilia (Ou et al., 2009). However, ACIII-deficient mice extend cilia of comparable lengths and remain able to traffic neuronal cilia receptors such as SSTR3 (Wang et al., 2009). Taken together, these data suggest that independent routes of protein trafficking to the cilium may underlie the developmental time course of receptor expression and cilium maturation.

In hippocampus, SSTR3 appears in cilia between ~P0 and ~P3 (Stanic et al., 2009), and, for neocortex, we previously observed SSTR3 in neonatal rat neocortex (Anastas et al., 2011). However, no studies are available on the development of SSTR3 localization in cilia in the neocortex. We must await further characterization of content and developmental appearance of other neuronal cilia receptors.

Neuronal cilia do not seem essential for proper neuronal migration or for acquisition of neuronal polarity

We observed that, in pyramidal neurons (Anastas et al., 2011; present data), the docking of the basal body generally forms on the pial side of the cell. However, in the major interneuron subtypes, PV^+ and CB^+ cells, the cilia/basal body seemed to be more randomly located on the soma. CR^+ cells, however, often exhibit a highly polarized morphology, and we found that the cilia could be in the “apical” dendrite. Overall, these data suggest that the positioning of the cilium might be related to the polarity of the neural cell type in that there is correlation between the docking location of the basal body and the relative position of the mother centriole as migration ceases. However, it seems that cilia formation is not essential for neuronal polarity or expression of layer-specific markers in neocortex. Despite a severe defect in ciliogenesis, analysis of mutant *Stumpy* mice revealed normal polarity of pyramidal neurons, with a well-developed apical dendrite. The preserved expression of laminar markers suggests that loss of cilia does not grossly disrupt timing of neuronal migration, which is consistent with our findings that cilia initiate growth postmigration. We cannot rule out that loss of cilia alters the fine positioning or morphology of cortical neurons. For example, we have observed subtle abnormalities in Purkinje cell position and morphology in the developing cerebellum of Δ*Stumpy* mice, but these changes could be secondary to granule cell dysgenesis or altered Sonic hedgehog signalling in the region (Breunig et al., 2008; Chizhikov et al., 2007; Spassky et al., 2008). Duplication of a neuron’s cilium number also does not seem to alter the general orientation of pyramidal neurons (Anastas et al., 2011; Sarkisian et al., 2001). Thus, dramatic changes to a neuron’s cilium do not grossly affect its position or morphology. Determining how or whether such mutations ultimately influence intracellular signalling pathways or connections between neurons requires further investigation.

Despite the increased attention given to this organelle, more precise genetic manipulations will be needed to assess the role of primary cilia in neurons definitively. Moreover, a proper

understanding of the dynamics of ciliogenesis will be needed to harness these technologies and to create informed hypotheses about these organelles. Our detailed description of the process of neuronal ciliogenesis will be useful for these endeavors and for future studies examining the significance and functional role of neuronal cilia.

Acknowledgments

Grant sponsor: National Institutes of Health; Grant number: DA02399 (to P.R.); Grant sponsor: National Institute of Neurological Disorders and Stroke; Grant number: NS038296-09 (to P.R.); Grant sponsors: Kavli Institute for Neuroscience (to P.R.); McKnight Brain Research Foundation and the Evelyn F. and William L. McKnight Brain Institute at the University of Florida (to M.R.S); Connecticut Stem Cell Research Grants Program (www.ct.gov/dph/cwp/view.aspa=3142&q=389702; to J.J.B.).

We thank Drs. Mladen-Roko Rasin and Nenad Sestan for providing us with EM-prepared tissue sections. We also thank Dr. Jill Verlander and George Kasnic of the University of Florida Core EM Facility, Doug Smith of the Cell and Tissue Analysis Core Facility, Dorit Siebzehnrubl, and Dr. Kirill Ukhanov for technical assistance.

LITERATURE CITED

Airaksinen MS, Eilers J, Garaschuk O, Thoenen H, Konnerth A, Meyer M. Ataxia and altered dendritic calcium signaling in mice carrying a targeted null mutation of the calbindin D28k gene. Proc Natl Acad Sci U S A. 1997; 94:1488–1493. [PubMed: 9037080]

Amador-Arjona A, Elliott J, Miller A, Ginbey A, Pazour GJ, Enikolopov G, Roberts AJ, Terskikh AV. Primary cilia regulate proliferation of amplifying progenitors in adult hippocampus: implications for learning and memory. J Neurosci. 2011; 31:9933–9944. [PubMed: 21734285]

Anastas SB, Mueller D, Semple-Rowland SL, Breunig JJ, Sarkisian MR. Failed cytokinesis of neural progenitors in citron kinase-deficient rats leads to multiciliated neurons. Cereb Cortex. 2011; 21:338–344. (Epub 2010, Jun 4). [PubMed: 20525772]

Barzi M, Berenguer J, Menendez A, Alvarez-Rodriguez R, Pons S. Sonic-hedgehog-mediated proliferation requires the localization of PKA to the cilium base. J Cell Sci. 2010; 123:62–69. [PubMed: 20016067]

Bearzatto B, Servais L, Roussel C, Gall D, Baba-Aissa F, Schurmans S, de Kerchove d'Exaerde A, Cheron G, Schiffmann SN. Targeted calretinin expression in granule cells of calretinin-null mice restores normal cerebellar functions. FASEB J. 2006; 20:380–382. [PubMed: 16352645]

Belgacem YH, Borodinsky LN. Sonic hedgehog signaling is decoded by calcium spike activity in the developing spinal cord. Proc Natl Acad Sci U S A. 2011; 108:4482–4487. [PubMed: 21368195]

Bennouna-Greene V, Kremer S, Stoetzel C, Christmann D, Schuster C, Durand M, Verloes A, Sigaudy S, Holder-Espinasse M, Godet J, Brandt C, Marion V, Danion A, Dietemann JL, Dollfus H. Hippocampal dysgenesis and variable neuropsychiatric phenotypes in patients with Bardet-Biedl syndrome underline complex CNS impact of primary cilia. Clin Genet. 2011 (E-pub 25 April 2011).

Berbari NF, Bishop GA, Askwith CC, Lewis JS, Mykytyn K. Hippocampal neurons possess primary cilia in culture. J Neurosci Res. 2007; 85:1095–1100. [PubMed: 17304575]

Berbari NF, Lewis JS, Bishop GA, Askwith CC, Mykytyn K. Bardet-Biedl syndrome proteins are required for the localization of G protein-coupled receptors to primary cilia. Proc Natl Acad Sci U S A. 2008; 105:4242–4246. [PubMed: 18334641]

Bishop GA, Berbari NF, Lewis J, Mykytyn K. Type III adenylyl cyclase localizes to primary cilia throughout the adult mouse brain. J Comp Neurol. 2007; 505:562–571. [PubMed: 17924533]

Brailov I, Bancila M, Brisorgueil MJ, Miquel MC, Hamon M, Verge D. Localization of 5-HT_6 receptors at the plasma membrane of neuronal cilia in the rat brain. Brain Res. 2000; 872:271–275. [PubMed: 10924708]

Breunig JJ, Sarkisian MR, Arellano JI, Morozov YM, Ayoub AE, Sojitra S, Wang B, Flavell RA, Rakic P, Town T. Primary cilia regulate hippocampal neurogenesis by mediating sonic hedgehog signaling. Proc Natl Acad Sci U S A. 2008; 105:13127–13132. [PubMed: 18728187]

Celio MR, Heizmann CW. Calcium-binding protein parvalbumin as a neuronal marker. Nature. 1981; 293:300–302. [PubMed: 7278987]

Celio MR, Baier W, Scharer L, Gregersen HJ, de Viragh PA, Norman AW. Monoclonal antibodies directed against the calcium binding protein Calbindin D-28k. Cell Calcium. 1990; 11:599–602. [PubMed: 2285928]

Chizhikov VV, Davenport J, Zhang Q, Shih EK, Cabello OA, Fuchs JL, Yoder BK, Millen KJ. Cilia proteins control cerebellar morphogenesis by promoting expansion of the granule progenitor pool. J Neurosci. 2007; 27:9780–9789. [PubMed: 17804638]

Cho YJ, Lee JC, Kang BG, An J, Song HS, Son O, Nam DH, Cha CI, Joo KM. Immunohistochemical study on the expression of calcium binding proteins (calbindin-D28k, calretinin, and parvalbumin) in the cerebral cortex and in the hippocampal region of nNOS knock-out(−/−) mice. Anat Cell Biol. 2011; 44:106–115. [PubMed: 21829754]

Cohen E, Binet S, Meininger V. Ciliogenesis and centriole formation in the mouse embryonic nervous system. An ultrastructural analysis. Biol Cell. 1988; 62:165–169. [PubMed: 3390625]

Dahl HA. Fine structure of cilia in rat cerebral cortex. Z Zellforsch Mikrosk Anat. 1963; 60:369–386. [PubMed: 14024614]

Davenport JR, Watts AJ, Roper VC, Croyle MJ, van Groen T, Wyss JM, Nagy TR, Kesterson RA, Yoder BK. Disruption of intraflagellar transport in adult mice leads to obesity and slow-onset cystic kidney disease. Curr Biol. 2007; 17:1586–1594. [PubMed: 17825558]

Defelipe J, Gonzalez-Albo MC, Del Rio MR, Elston GN. Distribution and patterns of connectivity of interneurons containing calbindin, calretinin, and parvalbumin in visual areas of the occipital and temporal lobes of the macaque monkey. J Comp Neurol. 1999; 412:515–526. [PubMed: 10441237]

Domire JS, Mykytyn K. Markers for neuronal cilia. Methods Cell Biol. 2009; 91:111–121. [PubMed: 20409783]

Domire JS, Green JA, Lee KG, Johnson AD, Askwith CC, Mykytyn K. Dopamine receptor 1 localizes to neuronal cilia in a dynamic process that requires the Bardet-Biedl syndrome proteins. Cell Mol Life Sci. 2010 (E-pub 9 December 2010).

Doxsey SJ, Stein P, Evans L, Calarco PD, Kirschner M. Pericentrin, a highly conserved centrosome protein involved in microtubule organization. Cell. 1994; 76:639–650. [PubMed: 8124707]

Dredge BK, Jensen KB. NeuN/Rbfox3 Nuclear and cytoplasmic isoforms differentially regulate alternative splicing and nonsense-mediated decay of Rbfox2. PLoS ONE. 2011; 6:e21585. [PubMed: 21747913]

Dubreuil V, Marzesco AM, Corbeil D, Huttner WB, Wilsch-Brauninger M. Midbody and primary cilium of neural progenitors release extracellular membrane particles enriched in the stem cell marker prominin-1. J Cell Biol. 2007; 176:483–495. [PubMed: 17283184]

Einstein EB, Patterson CA, Hon BJ, Regan KA, Reddi J, Melnikoff DE, Mateer MJ, Schulz S, Johnson BN, Tallent MK. Somatostatin signaling in neuronal cilia is critical for object recognition memory. J Neurosci. 2010; 30:4306–4314. [PubMed: 20335466]

Feng L, Cooper JA. Dual functions of Dab1 during brain development. Mol Cell Biol. 2009; 29:324–332. [PubMed: 18981215]

Ferland RJ, Cherry TJ, Preware PO, Morrisey EE, Walsh CA. Characterization of Foxp2 and Foxp1 mRNA and protein in the developing and mature brain. J Comp Neurol. 2003; 460:266–279. [PubMed: 12687690]

Fiala JC. Reconstruct: a free editor for serial section microscopy. J Microsc. 2005; 218:52–61. [PubMed: 15817063]

Fuchs JL, Schwark HD. Neuronal primary cilia: a review. Cell Biol Int. 2004; 28:111–118. [PubMed: 14984756]

Goetz SC, Anderson KV. The primary cilium: a signalling centre during vertebrate development. Nat Rev Genet. 2010; 11:331–344. [PubMed: 20395968]

Green JA, Mykytyn K. Neuronal ciliary signaling in homeostasis and disease. Cell Mol Life Sci. 2010; 67:3287–3297. [PubMed: 20544253]

Han YG, Spassky N, Romaguera-Ros M, Garcia-Verdugo JM, Aguilar A, Schneider-Maunoury S, Alvarez-Buylla A. Hedgehog signaling and primary cilia are required for the formation of adult neural stem cells. Nat Neurosci. 2008; 11:277–284. [PubMed: 18297065]

Handel M, Schulz S, Stanarius A, Schreff M, Erdtmann-Vourliotis M, Schmidt H, Wolf G, Hollt V. Selective targeting of somatostatin receptor 3 to neuronal cilia. Neuroscience. 1999; 89:909–926. [PubMed: 10199624]

Higginbotham HR, Gleeson JG. The centrosome in neuronal development. Trends Neurosci. 2007; 30:276–283. [PubMed: 17420058]

Jurczyk A, Pino SC, O'sullivan-Murphy B, Addorio M, Lidstone EA, Diiorio P, Lipson KL, Standley C, Fogarty K, Lifshitz L, Urano F, Mordes JP, Greiner DL, Rossini AA, Bortell R. A novel role for the centrosomal protein, pericentrin, in regulation of insulin secretory vesicle docking in mouse pancreatic beta-cells. PLoS ONE. 2010; 5:e11812. [PubMed: 20676397]

Kao HT, Li P, Chao HM, Janoschka S, Pham K, Feng J, McEwen BS, Greengard P, Pieribone VA, Porton B. Early involvement of synapsin III in neural progenitor cell development in the adult hippocampus. J Comp Neurol. 2008; 507:1860–1870. [PubMed: 18271024]

Kim J, Lee JE, Heynen-Genel S, Suyama E, Ono K, Lee K, Ideker T, Aza-Blanc P, Gleeson JG. Functional genomic screen for modulators of ciliogenesis and cilium length. Nature. 2010; 464:1048–1051. [PubMed: 20393563]

Kim KK, Adelstein RS, Kawamoto S. Identification of neuronal nuclei (NeuN) as Fox-3, a new member of the Fox-1 gene family of splicing factors. J Biol Chem. 2009; 284:31052–31061. [PubMed: 19713214]

Lee JH, Gleeson JG. The role of primary cilia in neuronal function. Neurobiol Dis. 2010; 38:167–172. [PubMed: 20097287]

LeVay S. Synaptic patterns in the visual cortex of the cat and monkey. Electron microscopy of Golgi preparations. J Comp Neurol. 1973; 150:53–85. [PubMed: 4124647]

Li A, Saito M, Chuang JZ, Tseng YY, Dedesma C, Tomizawa K, Kaitsuka T, Sung CH. Ciliary transition zone activation of phosphorylated Tctex-1 controls ciliary resorption, S-phase entry and fate of neural progenitors. Nat Cell Biol. 2011; 13:402–411. [PubMed: 21394082]

Lund JS, Boothe RG, Lund RD. Development of neurons in the visual cortex (area 17) of the monkey (*Macaca nemestrina*): a Golgi study from fetal day 127 to postnatal maturity. J Comp Neurol. 1977; 176:149–188. [PubMed: 410850]

Lyck L, Kroigard T, Finsen B. Unbiased cell quantification reveals a continued increase in the number of neocortical neurones during early post-natal development in mice. Eur J Neurosci. 2007; 26:1749–1764. [PubMed: 17897392]

Miyoshi K, Kasahara K, Miyazaki I, Asanuma M. Lithium treatment elongates primary cilia in the mouse brain and in cultured cells. Biochem Biophys Res Commun. 2009; 388:757–762. [PubMed: 19703416]

Morris RL, Scholey JM. Heterotrimeric kinesin-II is required for the assembly of motile 9 + 2 ciliary axonemes on sea urchin embryos. J Cell Biol. 1997; 138:1009–1022. [PubMed: 9281580]

Mullen RJ, Buck CR, Smith AM. NeuN, a neuronal specific nuclear protein in vertebrates. Development. 1992; 116:201–211. [PubMed: 1483388]

Murthy KS, Makhlouf GM. Differential coupling of muscarinic m2 and m3 receptors to adenylyl cyclases V/VI in smooth muscle. Concurrent M2-mediated inhibition via Galphai3 and m3-mediated stimulation via Gbetagammaq. J Biol Chem. 1997; 272:21317–21324. [PubMed: 9261144]

Nigg EA, Raff JW. Centrioles, centrosomes, and cilia in health and disease. Cell. 2009; 139:663–678. [PubMed: 19914163]

Ou Y, Ruan Y, Cheng M, Moser JJ, Rattner JB, van der Hoorn FA. Adenylate cyclase regulates elongation of mammalian primary cilia. Exp Cell Res. 2009; 315:2802–2817. [PubMed: 19576885]

Paxinos, G.; Franklin, KBJ. The mouse brain in stereotaxic coordinates. London: Academic Press; 2004.

Pazour GJ, Dickert BL, Vucica Y, Seeley ES, Rosenbaum JL, Witman GB, Cole DG. Chlamydomonas IFT88 and its mouse homologue, polycystic kidney disease gene tg737, are required for assembly of cilia and flagella. J Cell Biol. 2000; 151:709–718. [PubMed: 11062270]

Pedersen LB, Rosenbaum JL. Intraflagellar transport (IFT) role in ciliary assembly, resorption and signalling. Curr Top Dev Biol. 2008; 85:23–61. [PubMed: 19147001]

Pedersen LB, Veland IR, Schroder JM, Christensen ST. Assembly of primary cilia. Dev Dyn. 2008; 237:1993–2006. [PubMed: 18393310]

Poole CA, Jensen CG, Snyder JA, Gray CG, Hermanutz VL, Wheatley DN. Confocal analysis of primary cilia structure and colocalization with the Golgi apparatus in chondrocytes and aortic smooth muscle cells. Cell Biol Int. 1997; 21:483–494. [PubMed: 9451805]

Rasin MR, Gazula VR, Breunig JJ, Kwan KY, Johnson MB, Liu-Chen S, Li HS, Jan LY, Jan YN, Rakic P, Sestan N. Numb and Numbl are required for maintenance of cadherin-based adhesion and polarity of neural progenitors. Nat Neurosci. 2007; 10:819–827. [PubMed: 17589506]

Rooryck C, Pelras S, Chateil JF, Cances C, Arveiler B, Verloes A, Lacombe D, Goizet C. Bardet-Biedl syndrome and brain abnormalities. Neuropediatrics. 2007; 38:5–9. [PubMed: 17607597]

Saino-Saito S, Hozumi Y, Goto K. Excitotoxicity by kainate-induced seizure causes diacylglycerol kinase zeta to shuttle from the nucleus to the cytoplasm in hippocampal neurons. Neurosci Lett. 2011; 494:185–189. [PubMed: 21362459]

Sarkisian MR, Frenkel M, Li W, Oborski JA, LoTurco JJ. Altered interneuron development in the cerebral cortex of the flathead mutant. Cereb Cortex. 2001; 11:734–743. [PubMed: 11459763]

Sarkisian MR, Bartley CM, Chi H, Nakamura F, Hashimoto-Torii K, Torii M, Flavell RA, Rakic P. MEKK4 signaling regulates filamin expression and neuronal migration. Neuron. 2006; 52:789–801. [PubMed: 17145501]

Sfakianos J, Togawa A, Maday S, Hull M, Pypaert M, Cantley L, Toomre D, Mellman I. Par3 functions in the biogenesis of the primary cilium in polarized epithelial cells. J Cell Biol. 2007; 179:1133–1140. [PubMed: 18070914]

Sharma N, Berbari NF, Yoder BK. Ciliary dysfunction in developmental abnormalities and diseases. Curr Top Dev Biol. 2008; 85:371–427. [PubMed: 19147012]

Sharma N, Kosan ZA, Stallworth JE, Berbari NF, Yoder BK. Soluble levels of cytosolic tubulin regulate ciliary length control. Mol Biol Cell. 2011; 22:808–816.

Sorokin S. Centrioles and the formation of rudimentary cilia by fibroblasts and smooth muscle cells. J Cell Biol. 1962; 15:363–377. [PubMed: 13978319]

Sorokin SP. Centriole formation and ciliogenesis. Aspen Emphysema Conf. 1968; 11:213–216. [PubMed: 5751848]

Sotelo JR, Trujillo-Cenoz O. Electron microscope study on the development of ciliary components of the neural epithelium of the chick embryo. Z Zellforsch Mikrosk Anat. 1958; 49:1–12. [PubMed: 13625928]

Spassky N, Han YG, Aguilar A, Strehl L, Besse L, Laclef C, Ros MR, Garcia-Verdugo JM, Alvarez-Buylla A. Primary cilia are required for cerebellar development and Shh-dependent expansion of progenitor pool. Dev Biol. 2008; 317:246–259. [PubMed: 18353302]

Stanic D, Malmgren H, He H, Scott L, Aperia A, Hokfelt T. Developmental changes in frequency of the ciliary somatostatin receptor 3 protein. Brain Res. 2009; 1249:101–112. [PubMed: 18992731]

Stillman AA, Krsnik Z, Sun J, Rasin MR, State MW, Sestan N, Louvi A. Developmentally regulated and evolutionarily conserved expression of SLITRK1 in brain circuits implicated in Tourette syndrome. J Comp Neurol. 2009; 513:21–37. [PubMed: 19105198]

Town T, Breunig JJ, Sarkisian MR, Spilianakis C, Ayoub AE, Liu X, Ferrandino AF, Gallagher AR, Li MO, Rakic P, Flavell RA. The stumpy gene is required for mammalian ciliogenesis. Proc Natl Acad Sci U S A. 2008; 105:2853–2858. [PubMed: 18287022]

Tsai JW, Bremner KH, Vallee RB. Dual subcellular roles for LIS1 and dynein in radial neuronal migration in live brain tissue. Nat Neurosci. 2007; 10:970–979. [PubMed: 17618279]

Tucker RW, Pardee AB, Fujiwara K. Centriole ciliation is related to quiescence and DNA synthesis in 3T3 cells. Cell. 1979a; 17:527–535. [PubMed: 476831]

Tucker RW, Scher CD, Stiles CD. Centriole deciliation associated with the early response of 3T3 cells to growth factors but not to SV40. Cell. 1979b; 18:1065–1072. [PubMed: 229969]

Tury A, Mairet-Coello G, Dicicco-Bloom E. The cyclin-dependent kinase inhibitor p57Kip2 regulates cell cycle exit, differentiation, and migration of embryonic cerebral cortical precursors. Cereb Cortex. 2011; 21:1840–1856. [PubMed: 21245411]

Van Eden CG, Uylings HB. Cytoarchitectonic development of the prefrontal cortex in the rat. J Comp Neurol. 1985; 241:253–267. [PubMed: 2418068]

Waclaw RR, Ehrman LA, Pierani A, Campbell K. Developmental origin of the neuronal subtypes that comprise the amygdalar fear circuit in the mouse. J Neurosci. 2010; 30:6944–6953. [PubMed: 20484636]

Wang Y, Yin X, Rosen G, Gabel L, Guadiana SM, Sarkisian MR, Galaburda AM, Loturco JJ. Dcdc2 knockout mice display exacerbated developmental disruptions following knockdown of doublecortin. Neuroscience. 2011; 190:398–408. [PubMed: 21689730]

Wang Z, Li V, Chan GC, Phan T, Nudelman AS, Xia Z, Storm DR. Adult type 3 adenylyl cyclase-deficient mice are obese. PLoS ONE. 2009; 4:e6979. [PubMed: 19750222]

Wei J, Wayman G, Storm DR. Phosphorylation and inhibition of type III adenylyl cyclase by calmodulin-dependent protein kinase II in vivo. J Biol Chem. 1996; 271:24231–24235. [PubMed: 8798667]

Wei J, Zhao AZ, Chan GC, Baker LP, Impey S, Beavo JA, Storm DR. Phosphorylation and inhibition of olfactory adenylyl cyclase by CaM kinase II in neurons: a mechanism for attenuation of olfactory signals. Neuron. 1998; 21:495–504. [PubMed: 9768837]

Westra JW, Peterson SE, Yung YC, Mutoh T, Barral S, Chun J. Aneuploid mosaicism in the developing and adult cerebellar cortex. J Comp Neurol. 2008; 507:1944–1951. [PubMed: 18273885]

White EL, Rock MP. Three-dimensional aspects and synaptic relationships of a Golgi-impregnated spiny stellate cell reconstructed from serial thin sections. J Neurocytol. 1980; 9:615–636. [PubMed: 6160213]

Whitfield JF. The neuronal primary cilium—an extrasynaptic signaling device. Cell Signal. 2004; 16:763–767. [PubMed: 15115655]

Willaredt MA, Hasenpusch-Theil K, Gardner HA, Kitanovic I, Hirschfeld-Warneken VC, Gojak CP, Gorgas K, Bradford CL, Spatz J, Wolfl S, Theil T, Tucker KL. A crucial role for primary cilia in cortical morphogenesis. J Neurosci. 2008; 28:12887–12900. [PubMed: 19036983]

Wonders CP, Anderson SA. The origin and specification of cortical interneurons. Nat Rev Neurosci. 2006; 7:687–696. [PubMed: 16883309]

Wong ST, Trinh K, Hacker B, Chan GC, Lowe G, Gaggar A, Xia Z, Gold GH, Storm DR. Disruption of the type III adenylyl cyclase gene leads to peripheral and behavioral anosmia in transgenic mice. Neuron. 2000; 27:487–497. [PubMed: 11055432]

Xu H, He JH, Xiao ZD, Zhang QQ, Chen YQ, Zhou H, Qu LH. Liver-enriched transcription factors regulate micro-RNA-122 that targets CUTL1 during liver development. Hepatology. 2010; 52:1431–1442. [PubMed: 20842632]

Zimmermann L, Schwaller B. Monoclonal antibodies recognizing epitopes of calretinins: dependence on Ca^{2+}-binding status and differences in antigen accessibility in colon cancer cells. Cell Calcium. 2002; 31:13–25. [PubMed: 11990296]

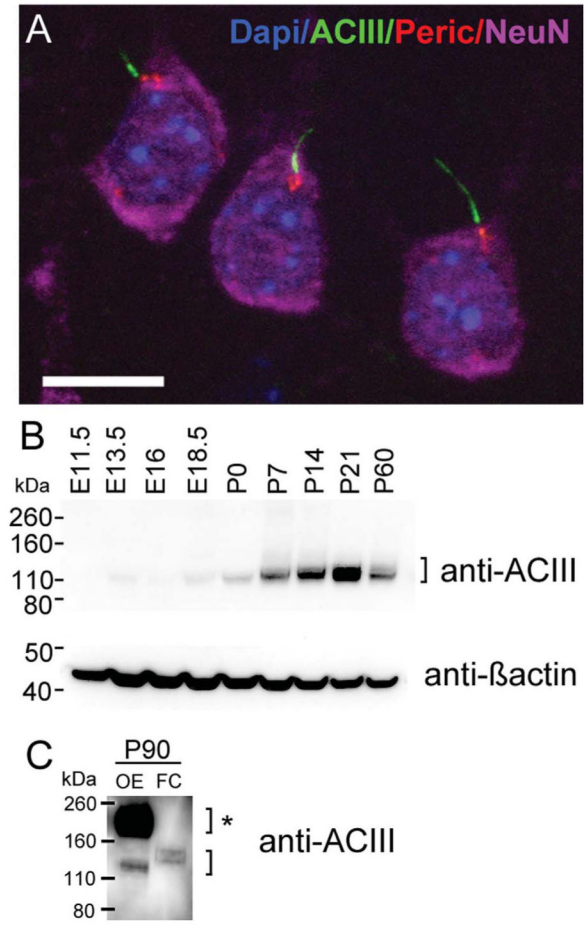

Figure 1.

Expression of adenylyl cyclase III during fetal and postnatal cortical development. **A:** Maximum intensity projection of a z-stack of layer 3 pyramidal neurons in the neocortex of a P90 mouse. Cilia were immunostained with ACIII (green), basal bodies with pericentrin (red), neuronal somata with NeuN (purple), and nuclei with DAPI (blue). **B:** Western blot detection of ACIII from mouse cortical lysates from embryonic day 11.5 (E11.5) to young adulthood (~P60). The upper blot for ACIII revealed a band close to the predicted MW of unglycosylated ACIII (MW of ~125 kDa). Generally, ACIII expression significantly increases between P0 and P21. At P60, there is a decrease in the intensity of the ACIII signal. β-Actin (lower blot) was used as a loading control. **C:** Protein lysates of P90 olfactory epithelium (OE) or frontal cortex (FC) were separated by Western blot and probed for ACIII. Very strong expression of ACIII is detected at ~190–200 kDa, which has been shown to reflect high levels of glycosylated ACIII (bracket with asterisk). This higher MW signal was absent in FC sample that revealed only a lower MW signal for ACIII (lower bracket). Scale bar = 10 μm.

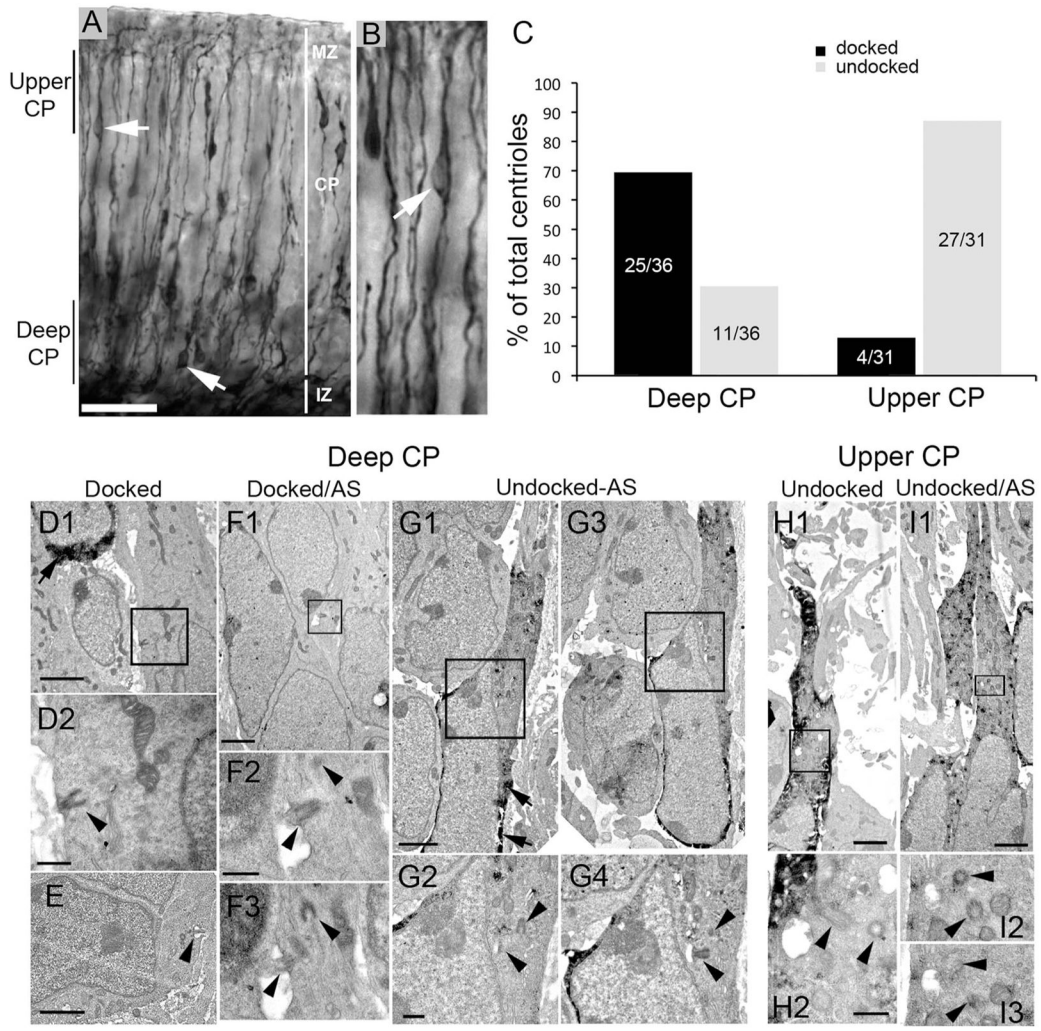

Figure 2.

Basal bodies are more prevalent in the deeper cortical plate (CP) at E16.5. E13.5 embryos electroporated with cDNA encoding GFP, killed and fixed for immuno-EM at E16.5. **A:** DAB immunostaining with anti-GFP antibodies shows GFP^+ cells (arrows) with leading and trailing processes in both the deeper layer and the upper layer of the CP. **B:** Higher magnification of the upper CP showing a cell (arrow) with a typical migrating profile. **C:** Bar graph shows a summary of the position of centrioles/basal bodies that were identified in deeper and upper layers of the CP docked (to the plasma membrane) or undocked. In deep CP, ~70% were docked (mostly in cells that were GFP^-). In upper CP, most centrioles (~90%) were undocked. **D–I:** Electron micrographic examples of centrioles and basal bodies in deep (D–G) or upper (H,I) CP. D1: A docked basal body in a GFP^- cell (boxed area is shown in D2). GFP immunoprecipitate is visible in the upper left cell (arrow). E: A docked basal body with a small axoneme extension (arrowhead). F1: Another example of a docked basal body in a GFP^- cell. The boxed region is shown in F2 and an adjacent section (AS) in F3. G1,3: Adjacent sections of a GFP^+ cell (arrows point to GFP precipitate) with a leading process. Boxed regions in G1,3 are magnified in G2,4, respectively. H1: A GFP^+ cell in the upper CP with undocked centrioles (boxed area is magnified in H2, which shows two centrioles (arrowheads). I1: Another example of a GFP^+ cell in the upper CP. The boxed

area in I1 is enlarged in I2, with an adjacent section shown in I3. Scale bars = 50 μm in A; 2 μm in D1,E,F1,G1,H1,I1; 0.5 μm in D2,F2,G2 H2.

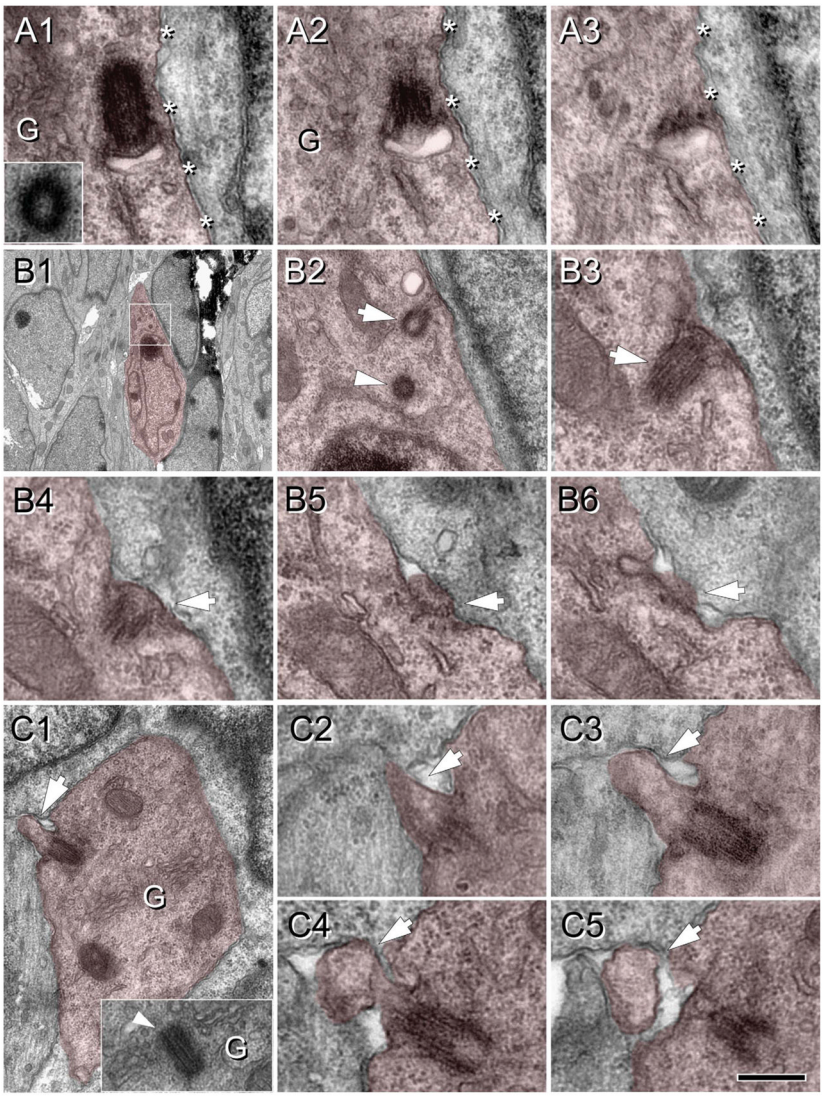

Figure 3.

Procilia in the fetal cortical plate at E16.5. Cells of interest and procilia are shaded to help identification. **A:** Serial sections (70 nm thick) illustrating an undocked mother centriole with an attached vesicle located adjacent to the cell membrane (asterisks). **Inset** in A1 shows the daughter centriole found in adjacent sections and (G) indicates Golgi cisterns around the centrosome. A2: A membranous centriolar protrusion, consistent with a procilium budding into the vesicle. This vesicular attachment is predictably the step before docking of the mother centriole to the cell membrane. **B:** Docked basal body with a protruding small procilium. B1: Low magnification image of the cell studied. Boxed area is magnified in B2. B2: Detail of the mother centriole (arrow) and the daughter centriole (arrowhead) located between the nucleus and the pial oriented process. B3–6: Serial sections (70 nm thick) illustrating the short procilium (~0.1 μm long) protruding from the attached mother centriole (arrow). **C:** Docked basal body with developed procilium. C1: Low magnification image of the cell analyzed showing the procilium (~0.3 μm long; arrow) protruding outside the cell. **Inset** shows an adjacent section illustrating the centriole surrounded by Golgi cisterns. C2–5: Serial sections (70 nm thick) illustrating the extent and mushroom shape of the procilium (arrow). Scale bar = 0.25 μm in C5 (applies to A,B3–6,C2–5); 3.6 μm for B1; 0.5 μm for

B2; 0.54 μm for C1. [Color figure can be viewed in the online issue, which is available at wileyonlinelibrary.com.]

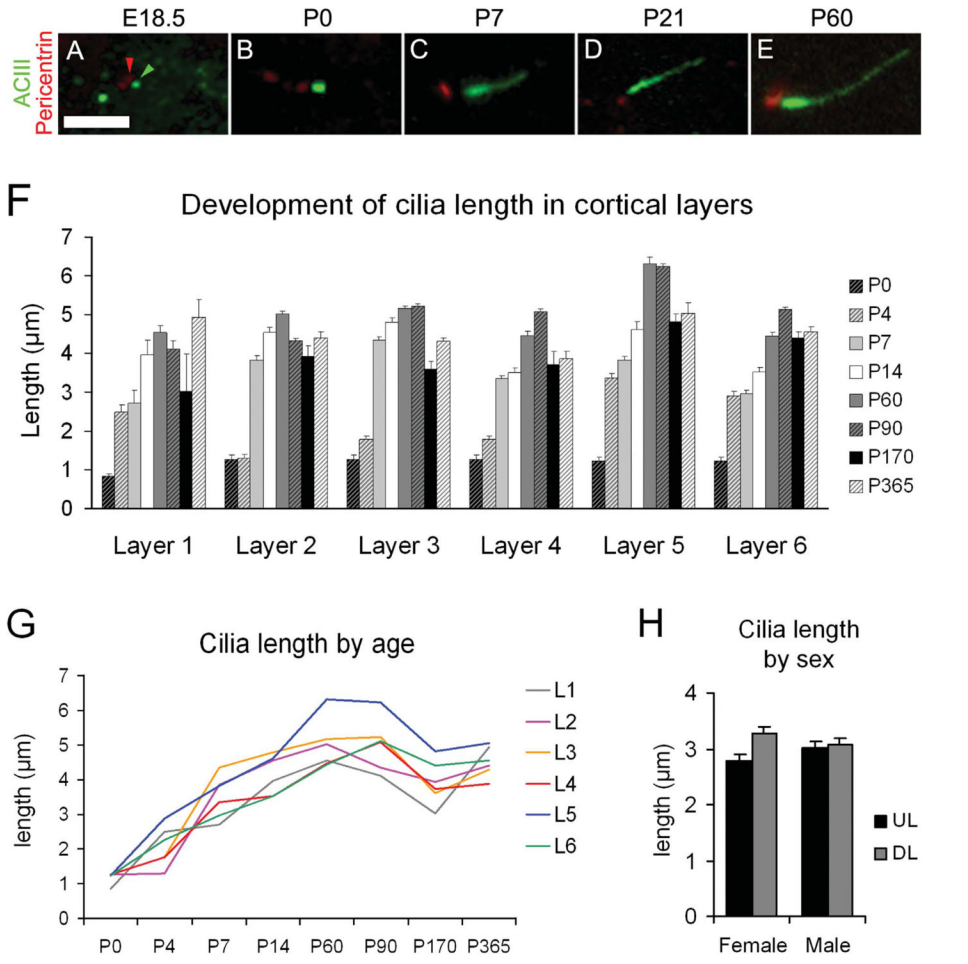

Figure 4.

Elongation of neuronal cilia over several postnatal weeks. **A–E:** Examples of basal bodies (pericentrin^{+}; red; example indicated by red arrowhead) and cilia (ACIII^{+}; green; example indicated by green arrowhead) for the indicated ages. **F:** Bar graph shows the average ± SEM of cilia length (μm) in the neocortical layers at the indicated ages. Because it was difficult to differentiate neocortical lamina at early ages, average lengths for layers 2–4 and layers 5–6 were pooled for P0, whereas at P4 layers 3 and 4 were also pooled. **G:** Graphic representation of cilia elongation across age in the cortical layers. Mean values of length are used (SEM values are omitted for clarity but can be found in Table 2). **H:** Comparison of cilia length in upper layers (2–4; UL) and deep layers (5–6; DL) of the neocortex in male and female P14 mice did not show significant effect of gender. Scale bar = 2.5 μm.

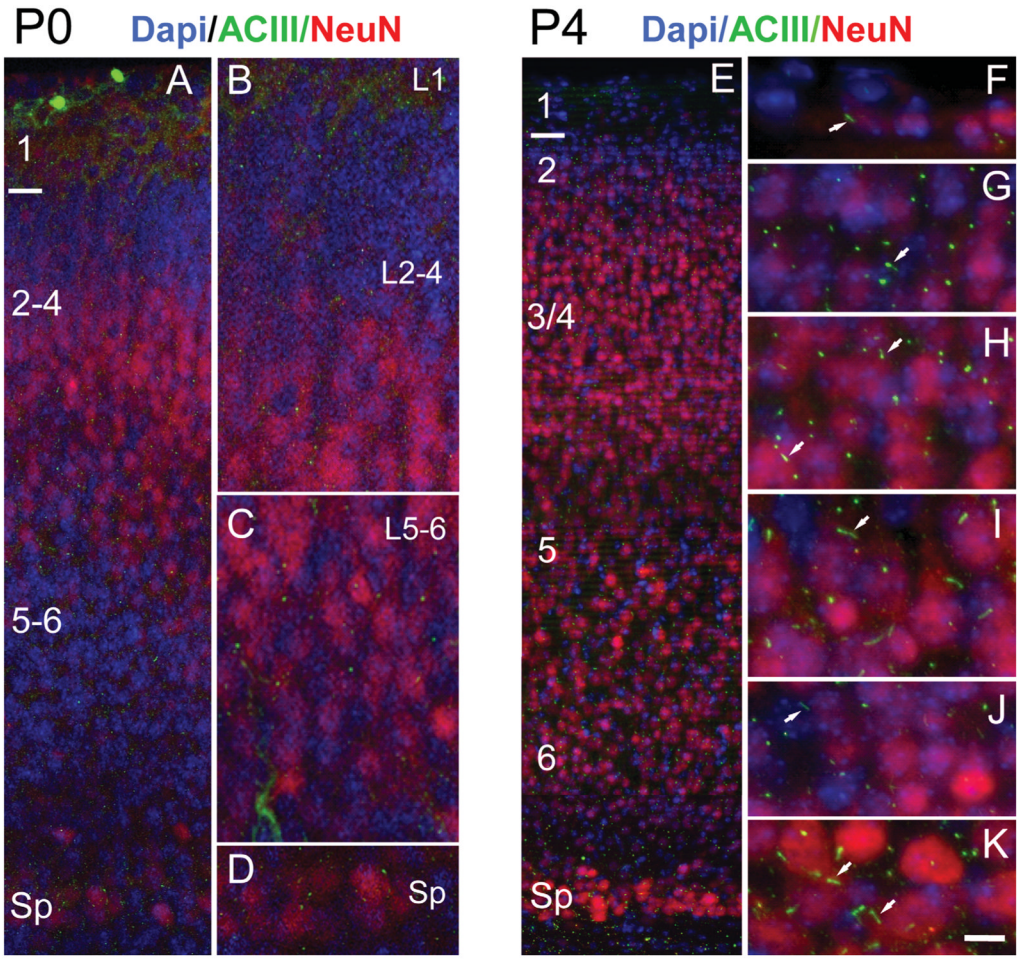

Figure 5.

Distribution of procilia in the neocortex at P0 and P4. **A:** Low-magnification view of the P0 neocortex immunostained for ACIII (green) and NeuN (red) and counterstained with DAPI (blue). NeuN is expressed in some cells of layers 2–5, scarce cells in layer 6, and intensely by some cells in the subplate (Sp). **B–D:** Details of the neocortex illustrating approximate layers 1–4 (L1, L2–4) in B, layers 5 and 6 (L5–6) in C, and the Sp in D. $ACIII^{+}$ specks were found in all layers, with rare longer, rod-shaped cilia. **E:** Low-magnification view of the P4 neocortex immunostained for ACIII and NeuN and counterstained with DAPI. **F–K:** High-magnification details of the cortical layers from layer 1 to the Sp. NeuN is still not fully expressed by all neurons, and layer 2 (G) and deep layer 6 (J) have few stained neurons. In contrast, the subplate (K) shows large neurons intensely stained with NeuN. Overall, intense $ACIII^{+}$ puncta are predominant, although scattered longer cilia can be found in all layers (arrows) and particularly in some neurons in layer 5 (I) and in the Sp (K). Scale bar = 10 μm in K (applies to F–K); 15 μm for A; 8 μm for B–D; 30 μm for E.

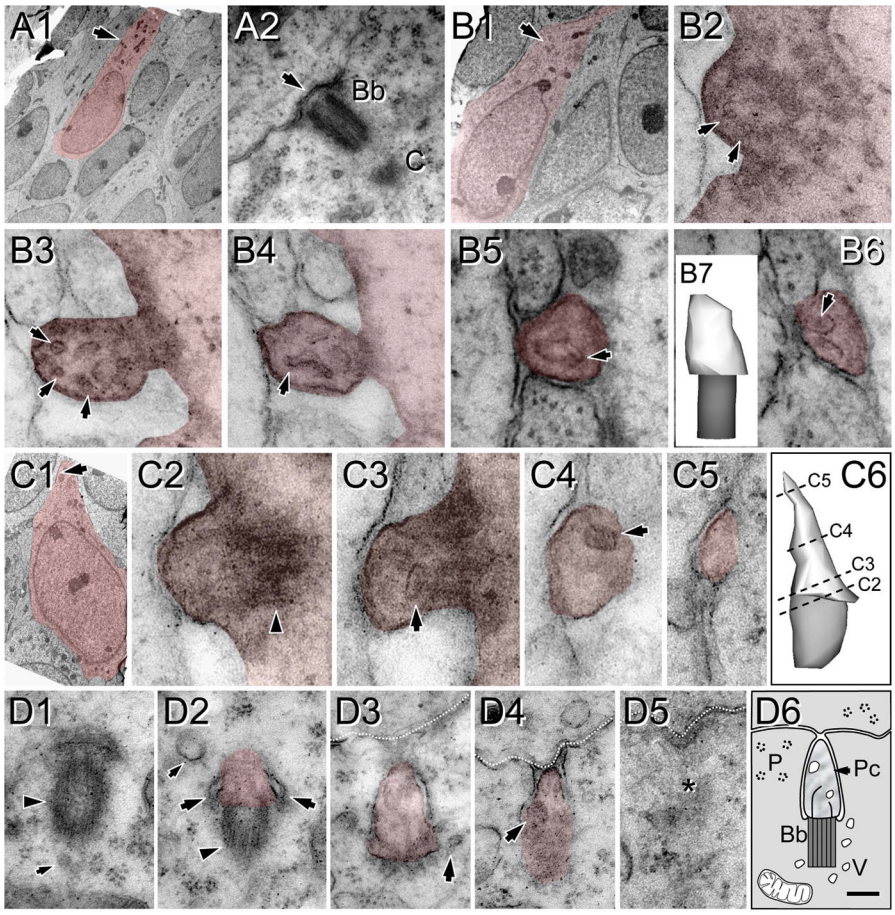

Figure 6.

Heterogeneity of procilia at P0 in the upper cortical plate. Cells and procilia of interest are shaded to help with identification. **A1:** Low-magnification view of a cell with neuronal morphology in layer 2; arrow indicates the position of the docked centriole (basal body). **A2** shows higher magnification of the basal body (Bb) and part of the adjacent daughter centriole (C). Note the lack of procilium (arrow) that was also absent in adjacent serial sections. **B:** A procilium in a cell with neuronal morphology in layer 2. B1: Low-magnification view of the cell with an arrow indicating the location of the procilium. B2: Cross-section of the basal body showing microtubular doublets (arrows) in the transitioning basal body/axonemal rudiment. B3–6: Serial sections (70 nm) through the procilium show the lack of axoneme but the presence of a tubular/vesicular network (arrows) inside the procilium. B7: 3D reconstruction of the procilium (white) and basal body (gray). **C:** Procilium in a cell with neuronal morphology. C1: Low-magnification view of a cell with an arrow indicating the location of the procilium. C2: Transition between the basal body (arrowhead) and procilium. C3–5: Serial sections illustrate a short procilium lacking microtubules and containing some vesicular structures (arrows). C6: 3D reconstruction of the basal body (gray) and the procilium (white) indicating the levels of C2–5 sections. **D:** Serial sections showing a procilium growing inside the cytoplasm in a cell in the upper cortical plate. D1: The basal body (arrowhead) and an adjacent vesicle (small arrow). D2: The basal body (arrowhead) and the budding procilium with a vesicle attached (large arrows). D3,4: The procilium is surrounded by the cell membrane and reaching the extracellular space in contact with an adjacent cell (discontinuous white line). Vesicles in and around the procilium are indicated with arrows. D5: Final section containing the

procilium (asterisk). D6: Schematic of the procilia (Pc) growing inside the cytoplasm. Bb, basal body; V, vesicles; P, polyribosomes. Scale bar = 90 nm in D6 (applies to D1–5); 4 μm for A1; 0.18 μm for A2; 3 μm for B1; 70 nm for B2–6,C2–5; 0.15 μm for B7; 2 μm for C1; 0.1 μm for C6.

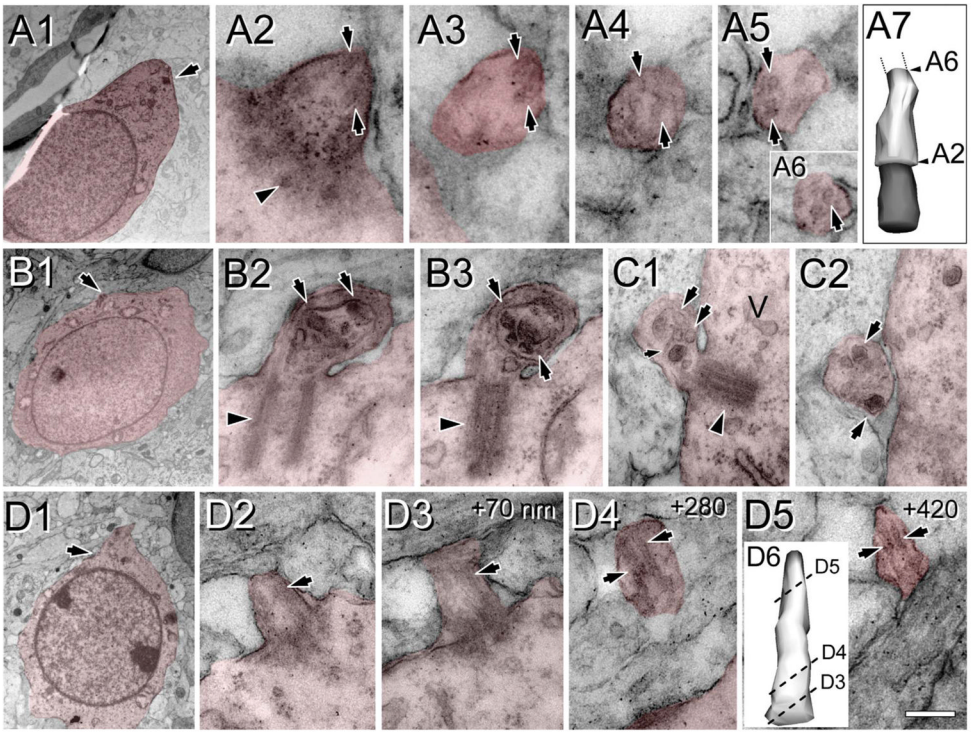

Figure 7.

Procilia in the deep cortical plate at P0. Cells and procilia of interest are shaded to help with identification. **A1:** Low-magnification view of a cell with neuronal morphology bearing a procilium (arrow) in its pial aspect. **A2–6:** Serial sections of the procilium from the cell in A1. A2: The transition between the basal body (arrowhead) to the procilium. The procilium lacks an axoneme, but some microtubule-like structures are detectable (arrows in A2–6). **A7:** 3D reconstruction of the basal body (gray) and the (incomplete) procilium (white) indicating the relative positions of sections A2 and A6. **B:** Procilium in the deep cortical plate with “cabbage-like” morphology. B1: Low-magnification image of the cell with neuronal morphology bearing the procilium. B2,3: Serial micrographs showing the basal body (arrowhead) and the procilium with membrane foldings and multiple vesicles (arrows). **C:** Another example of a procilium containing multiple vesicles (arrows) and occasional tubular structures (small arrow). Vesicles (V) were also frequent around the basal body (arrowhead in C1). **D:** A cilium with axoneme in a cell with neuronal morphology in the subplate. D1: Low-magnification image of the cell bearing the cilium (arrow). D2–5: Selected serial oblique sections of the cilium illustrating the presence of parallel microtubules (arrows) forming the axoneme. The distance (nanometers) between sections is indicated at upper right. Surprisingly, the microtubules are more visible in distal sections (D4,5) than in proximal ones (D2,3). D6: 3D reconstruction of the cilium (basal body is not illustrated) showing the levels of sections D3–5. Scale bar = 0.16 μm in D5 (applies to D4,5); 2 μm for A1,B1; 90 nm for A2–6, 0.26 μm for A7; 0.18 μm for B2–3; 0.24 μm for C1,2; 1.8 μm for D1; 0.2 μm for D2,3; 0.25 μm for D6. [Color figure can be viewed in the online issue, which is available at wileyonlinelibrary.com.]

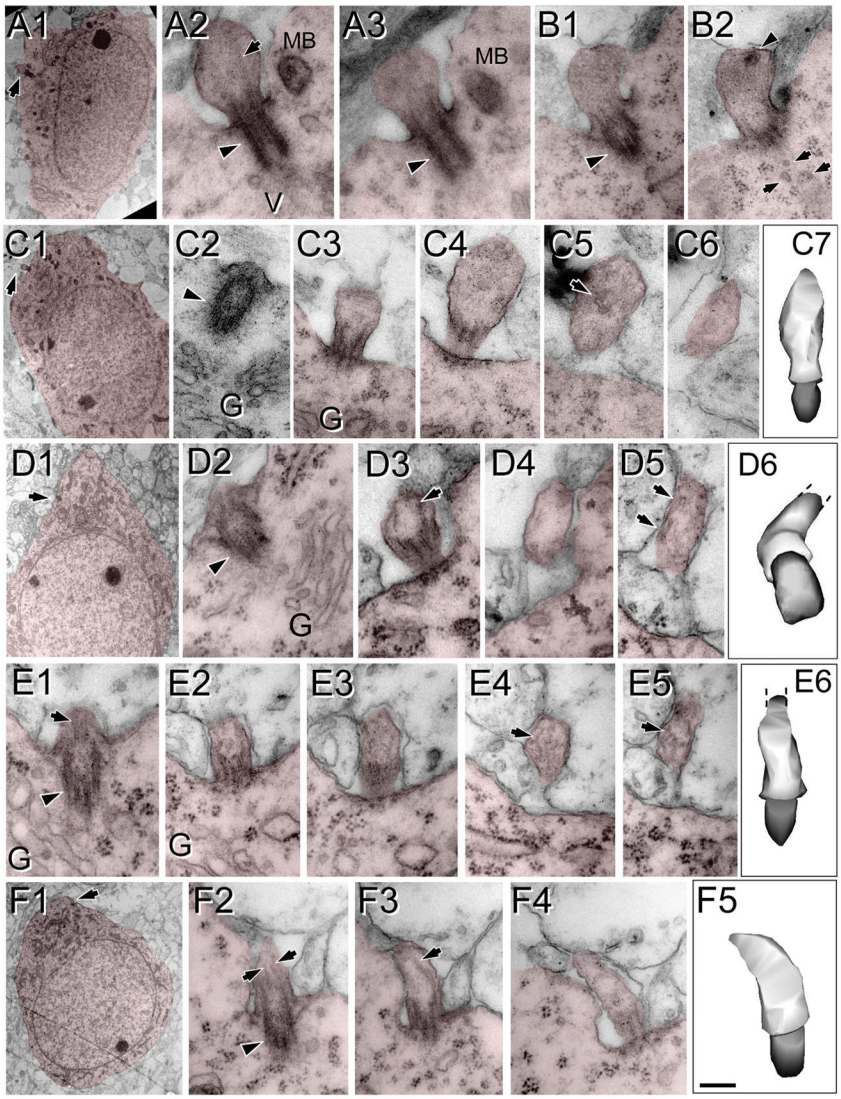

Figure 8.

Procilia in P4 neocortex. Cells of interest and procilia are shaded to help with identification. Illustrated are examples of procilia lacking axonemes (A–C) and procilia located in the deep cortical plate with some microtubular structures but lacking a well-formed axoneme (D–F). **A–C:** Enlarged, apparently immature procilia, present both in the deep (A) and in the superficial (B,C) cortical plate. A1: Low-magnification view of a cell with neuronal morphology in the deep cortical plate; the arrow indicates the location of the procilium. A2,3: Serial longitudinal sections along the basal body (arrowhead) and procilium containing some microtubules (arrow). A multivesicular body (MB) and vesicles (V) could be found in the vicinity. B: Serial longitudinal sections along the basal body (arrowhead in B1) and stubby procilium containing a dark structure (arrowhead in B2). Vesicles (arrows in B2) were common close to the basal body. C1: Low-magnification view of a cell with neuronal morphology located in the deep cortical plate; the arrow indicates the location of the procilium. C2–6: Serial oblique sections through the basal body (arrowhead) and procilium (C3–6) containing vesicle-like structures (arrow in C5). C7: 3D reconstruction of the basal body (gray) and the cilium (white). **D–F:** Examples of procilia containing microtubule-like structures. D1: Low-magnification view of a cell with neuronal

morphology located in the deep cortical plate; the arrow indicates the location of the procilium. D2–5: Serial sections (70 nm thick) through the procilium. D2: The basal body (arrowhead) and the adjacent Golgi apparatus (G). D3–5: Oblique sections through the procilium showing lack of axoneme with presence of scattered tubular structures (arrows). D6: 3D reconstruction of the basal body (gray) and the cilium (white). E1–6: Serial longitudinal sections along the basal body (arrowhead in E1) and the procilium containing disorganized microtubules (arrows). Golgi apparatus (G) vesicles were located close to the basal body. E6: 3D reconstruction of the basal body (gray) and the cilium (white). F1: Low-magnification view of the cell with neuronal morphology; the arrow indicates the location of the procilium. F2–5: Serial longitudinal sections along the basal body (arrowhead in F2) and the procilium that contains a few microtubules in a parallel arrangement (arrows), compatible with a developing axoneme. F5: 3D reconstruction of the basal body (gray) and the cilium (white). Scale bar = 0.2 μm in F5 (applies to F2–5); 2 μm for A1,C1,F1; 0.18 for A2,3,B1,2,C2–6,D6,E1–5; 0.25 for C7; 3 μm for D1; 0.16 μm for D2–5; 0.22 for E6. [Color figure can be viewed in the online issue, which is available at wileyonlinelibrary.com.]

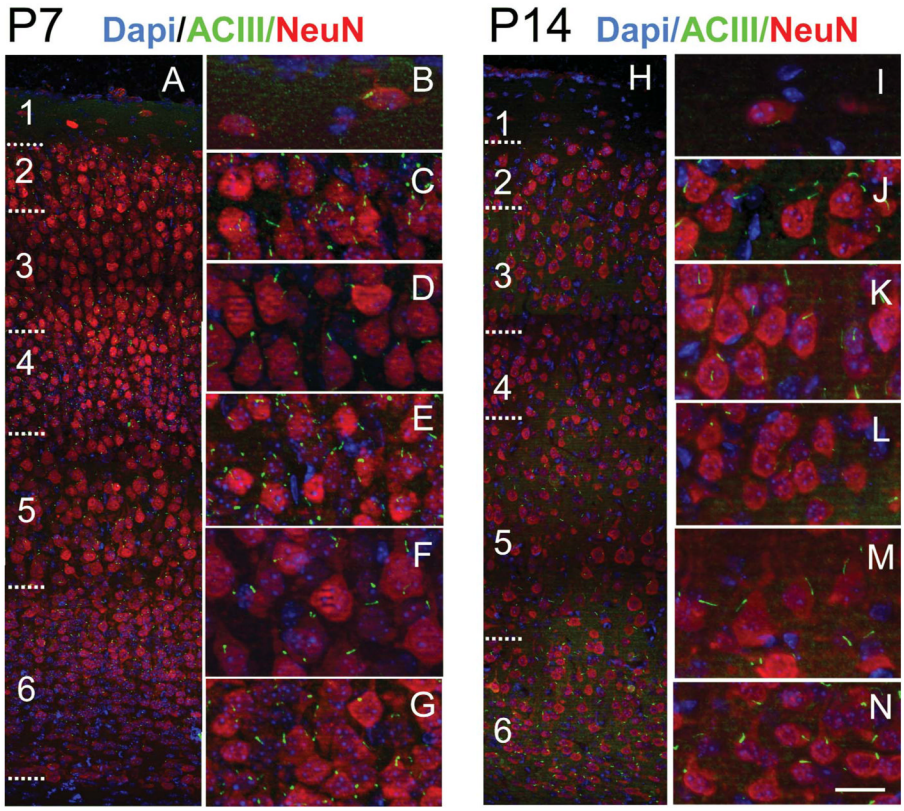

Figure 9.

ACIII^{+} cilia extend from neurons in all lamina of neocortex at P7 and P14. **A:** Low-magnification view of P7 neocortex immunostained for ACIII (green) and NeuN (red) and counterstained with DAPI (blue). **B–G:** High-magnification views of layers 1 (B), 2 (C), 3 (D), 4 (E), 5 (F), and 6 (G). Compared with P4 (Fig. 5), layers are more developed, neuropil is expanding, and cilia are longer and growing at similar rates in all layers (see Table 2). **H–N:** Low-magnification view of P14 neocortex immunostained for ACIII and NeuN and counterstained with DAPI. High-magnification views of layers 1 (I), 2 (J), 3 (K), 4 (L), 5 (M), and 6 (N) are shown at right. Note the expansion of the neuropil and more elongated appearance of cilia in all layers. At this age, cilia lengths reach ~70–90% of maximal lengths (see Table 2). Scale bar = 20 μm in N (applies to I–N); 70 μm for A; 24 μm for B–G; 70 μm for H.

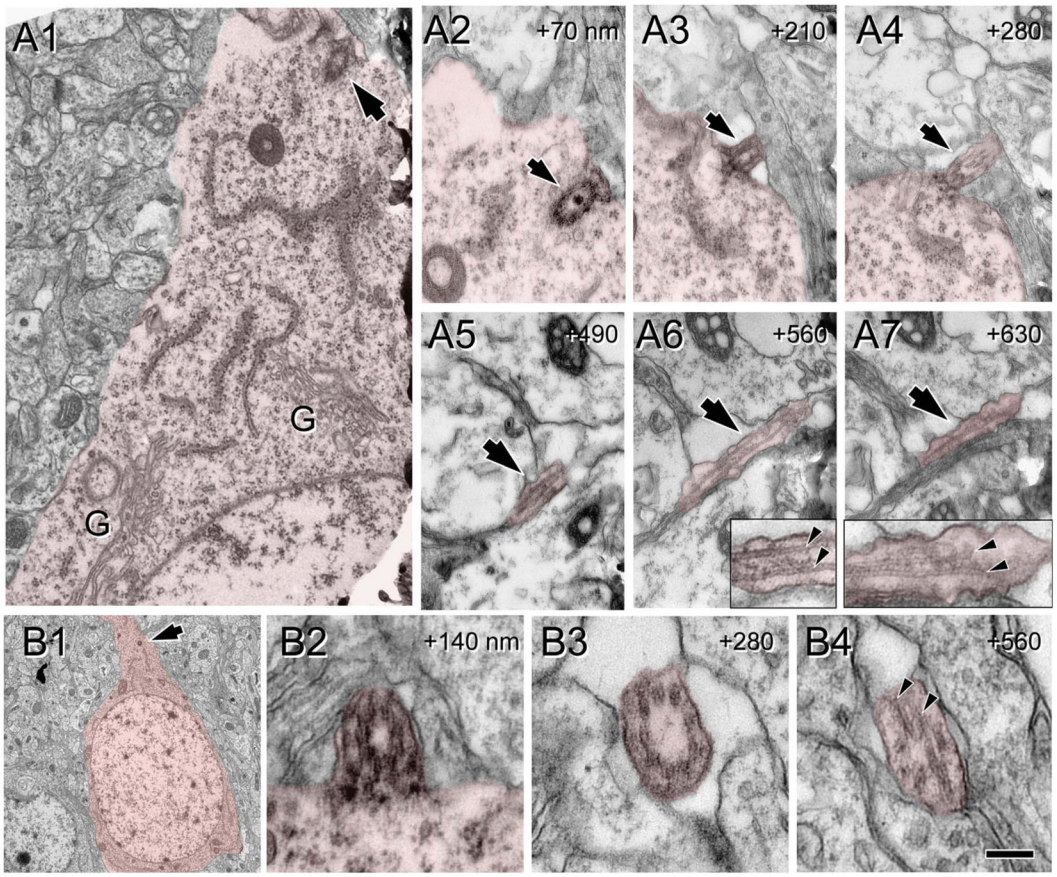

Figure 10.

Ultrastructure of cilia at P8. Cells of interest and procilia are shaded to help with identification. **A:** Serial micrographs of a cilium at P8. A1: Panoramic view of the cytoplasm and initial apical dendrite of a pyramidal neuron with the basal body attached to the membrane (arrow). G, Golgi apparatus. A2–7: Serial sections of the cilium (arrow) protruding outside of the cell. Well-formed and structured microtubules in the proximal segment (**insets** in A6,7) appear disorganized distally (inset in A7). Numbers in upper right corner indicate the Z distance between sections in nanometers. **B:** Serial sections of a cilium from a pyramidal neuron at P8. B1: Panoramic view of the pyramidal cell. Cilium location is indicated (arrow). B2–4: Serial micrographs of the cilia from neuron in B1. B2 illustrates the transition between the basal body and the cilium, and B3,4 are transverse and oblique sections through the cilium showing a straight morphology and a well-developed axoneme along the available length of 0.56 μm. Vesicles were less frequent at this age. Scale bar = 0.12 μm in B4 (applies to B2–4); 0.5 μm for A1; 0.4 μm for A2–7; 5 μm for B1. [Color figure can be viewed in the online issue, which is available at wileyonlinelibrary.com.]

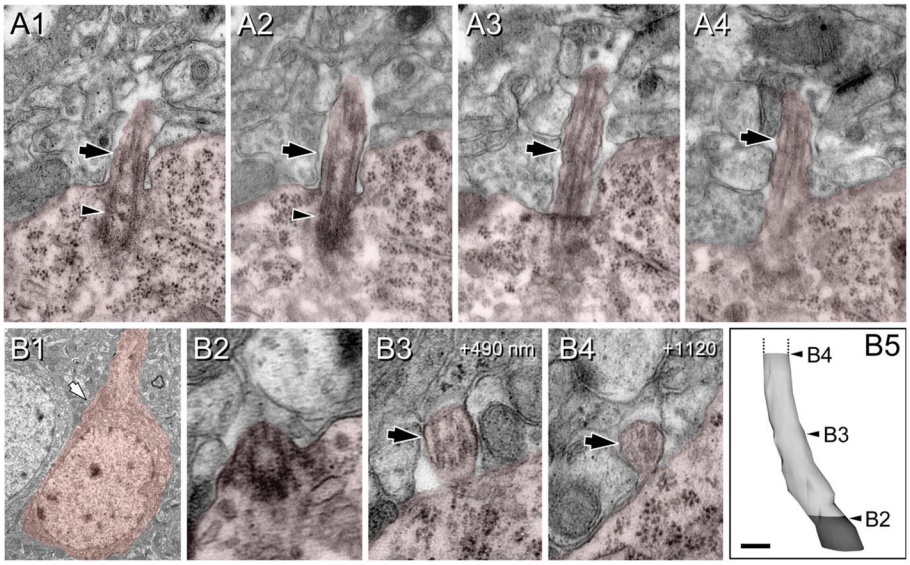

Figure 11.

Ultrastructure of cilia at P60. Cells of interest and procilia are shaded to help with identification. **A:** Serial sections along the basal body (arrowhead) and proximal segment (arrow) of a neuronal cilium. Notice the well-developed microtubules. **B:** Serial transverse sections of a pyramidal cell cilium (incomplete). B1: Panoramic view of a pyramidal neuron. Location of the cilium is indicated (arrow). B2–4: Details of transverse sections through the cilium of the pyramidal neuron in B1. B2: Transition basal body-cilium. B3: Middistance of the series. B4: Final section at about 1.2 μm from the origin. Note the rounded shape of the ciliar membrane and the well-developed axoneme along the available length. B5: 3D reconstruction of the basal body (gray) and the (incomplete) cilium (white). Positions of images B2–4 are indicated. Numbers in upper right corner indicate the Z distance to the cilium origin in nanometers. Scale bar = 0.18 μm in B5; 0.17 μm for A; 1.5 μm for B1; 0.1 for B2–4. [Color figure can be viewed in the online issue, which is available at wileyonlinelibrary.com.]

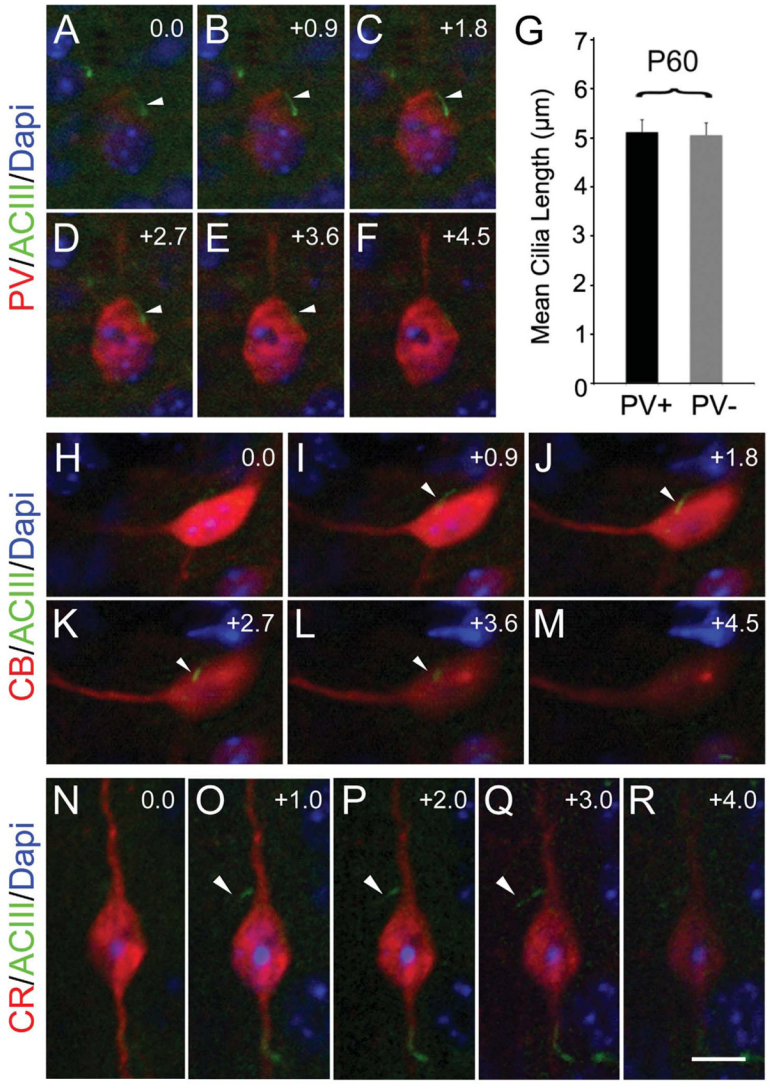

Figure 12.

Different interneuron subtypes in neocortex extend cilia. Examples of ciliated interneurons in the neocortex of P60 mice. **A–F:** An ACIII^{+} (arrow) cilium extending out of a parvalbumin (PV)-positive cell. **G:** Bar graph shows cilia length between PV^{+} and neighboring PV^{-} cells were comparable (~5 μm). **H–M:** Example of a calbindin (CB)-positive interneuron with an ACIII^{+} cilium (arrow). **N–R:** A calretinin (CR)-positive interneuron extending an ACIII^{+} cilium (arrow). Interestingly, some bipolar CR^{+} cells extended their cilia from the proximal part of the ascending (pial-oriented) dendrite, as illustrated. Numbers in the right upper corner of images indicate z-step increments in micrometers. Scale bar = 7.5 μm in R (applies to N–R); 12 μm for A–F; 10 μm for H–M.

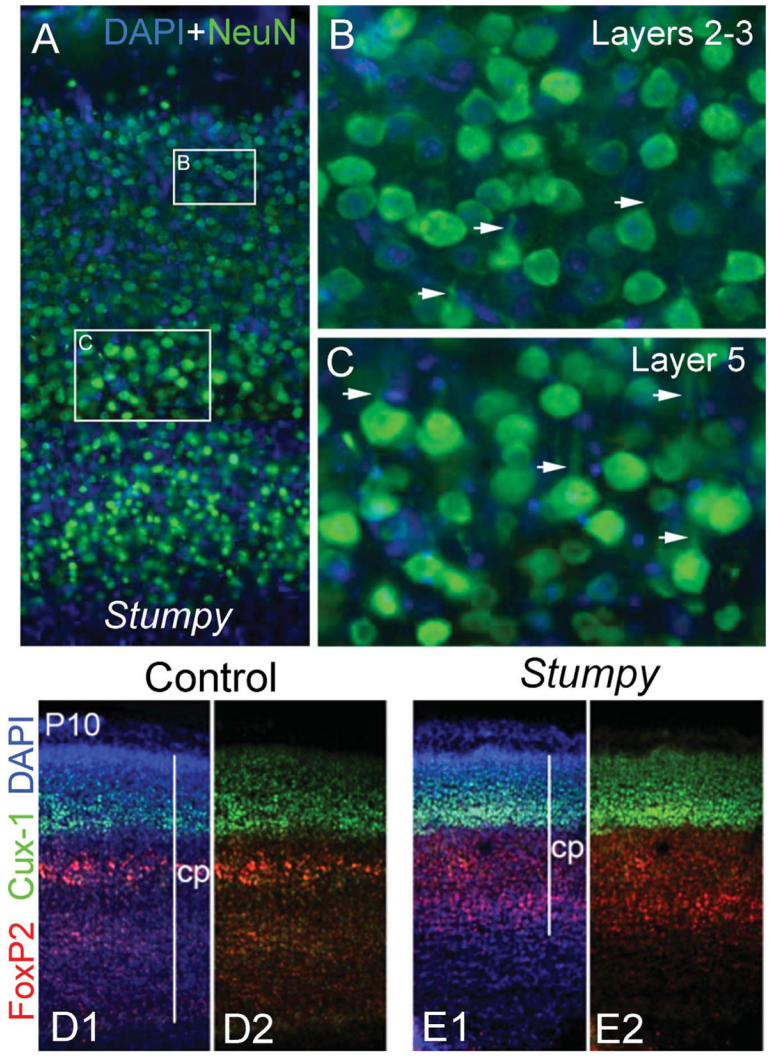

Figure 13.

Mutants lacking cilia show normal gross cytoarchitecture. **A:** Panoramic view of the neocortex of Δ*Stumpy* mutant mice immunostained for NeuN (green) and counterstained with DAPI (blue). The boxed areas in A represent higher magnification views of layers 2–3 (**B**) and 5 (**C**). In spite of the cortical compression resulting from hydrocephalus, Δ*Stumpy* mice lacking cilia exhibit normal polarization in pyramidal neurons, with well-formed and oriented apical dendrites (arrows in B,C). **D,E:** Panoramic view of the cortical plate (cp) of P10 control (D1,2) and Δ*Stumpy* mice (E1,2) immunostained for Cux1 (upper layer neurons marker; green) and Foxp2 (deeper layer neurons marker; red). Stratification of cortical layers was also grossly preserved in mice lacking cilia. D2 and E2 have had the DAPI channel removed.

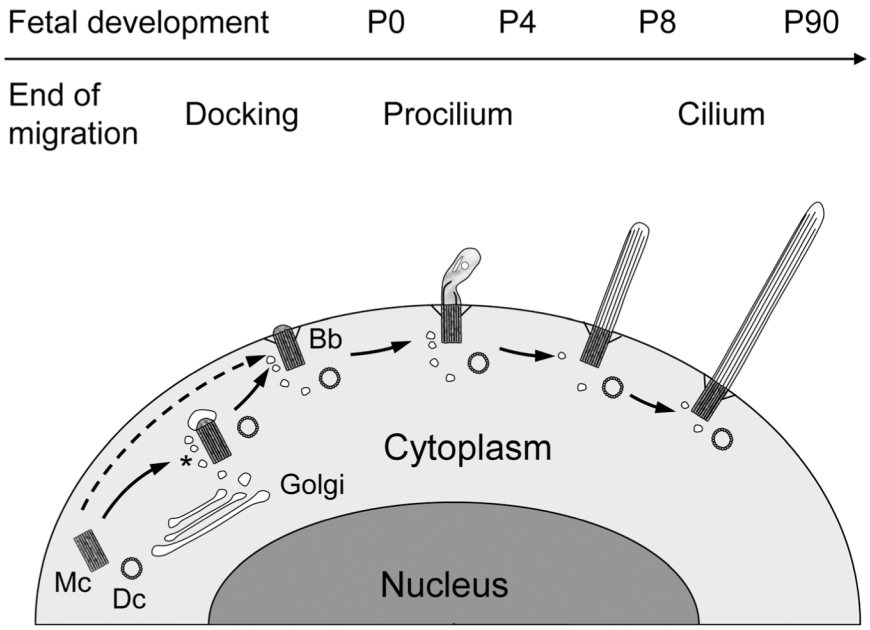

Figure 14.

Model of ciliogenesis stages in mouse neocortical neurons. We propose the following model. Migrating neurons do not bear cilia; rather, their mother centriole (Mc) and daughter centriole (Dc) are free in the cytoplasm. Once cells terminate migration and reach their appropriate lamina, the mother centriole attaches a vesicle, likely from the Golgi apparatus, buds a very short procilium and docks to the plasma membrane. It is also possible that the mother centriole docks directly to the plasma membrane without vesicle attachment as indicated by the dashed arrow. Docking to the membrane involves developing specific structures such as transition filaments, and the mother centriole will become a basal body (Bb), frequently surrounded by vesicles (asterisk). This basal body will grow the procilium, a membranous expansion about 0.5–2 μm in length, whose main feature is the lack of proper axoneme and that typically contains vesicles, short and disorganized tubular structures, and electron-dense diffuse content. This procilium does not display typical axonemal characteristics until ~P8, although axonemal growth seems to start at ~P0 in some subplate cells and could start ~P4 in some populations of neurons that showed early elongation of cilia (e.g., some layer 5 neurons). Overall, cilia will take weeks to elongate fully toward a peak at ~P60–P90, with some differences between layers.

TABLE 1

Primary Antibodies Used in This Study[1]

Antigen	Immunizing antigen	Manufacturer details	Working dilution
Adenylyl cyclase III (ACIII)	Synthetic peptide with the C-terminal 20 amino acids of mouse ACIII (PAAFPNGSSVTLPHQVVDNP)	Santa Cruz Biotechnology; catalog No. sc-588; rabbit polyclonal	1:1,000 (WB) 1:1,000 (IHC)
β-Actin	A modified β-cytoplasmic actin N-terminal peptide (DDDIAALVIDNGSGK, conjugated to KLH)	Sigma; catalog No. A5316; mouse monoclonal	1:10,000 (WB)
Calbindin-D28K	Calbindin D-28k purified from chicken gut	Swant; catalog No. 300; mouse monoclonal	1:4,000 (IHC)
Calretinin	Recombinant human calretinin-22k	Swant; catalog No. 6B3; mouse monoclonal	1:2,000 (IHC)
Green fluorescent protein (GFP)	Recombinant full-length GFP	Abcam; catalog No. ab13970; chicken polyclonal	1:5,000 (IHC) 1:1,000 (IHC)
Neuronal nuclear protein (NeuN)	Cell nuclei purified from mouse brain	Chemicon; catalog No. MAB377; mouse monoclonal	1:1,000 (IHC)
Parvalbumin	Purified parvalbumin from carp muscle	Swant; catalog No. 235; mouse monoclonal	1:4,000 (IHC)
Class IIIβ tubulin (Tuj1)	Purified microtubules from rat brain	Covance; catalog No. MMS-435P mouse monoclonal	1:1,250 (IHC)
Pericentrin	A fusion protein containing T7-Gene10 and ~60kD of pericentrin (amino acids 870–1370 of the mouse protein).	Covance; catalog No. PRB-432C; rabbit polyclonal	1:500 (IHC)
Pericentrin	Amino acids 1692–1814 of mouse pericentrin	BD Biosciences; catalog No. 611815; mouse monoclonal	1:200 (IHC)
Cux-1	Amino acids 1111–1332 of mouse CDP (CCAAT displacement protein)	Santa Cruz Biotechnologies; catalog No. sc-13024; rabbit polyclonal	1:100 (IHC)
FOXP2	Synthetic peptide: REIEEEPLSEDLE, corresponding to amino acids 703–715 of human FOXP2	Abcam; catalog No. ab1307; goat polyclonal	1:100 (IHC)

[1]WB, Western blot; IHC, immunohistochemistry.

TABLE 2

Average Length of Cilia in the Neocortical Lamina at Different Ages[1]

	L1	L2	L3	L4	L5	L6
P0	0.9 ± 0.1 (2)	1.3 ± 0.1 (3.3)	1.3 ± 0.1 (3.3)	1.3 ± 0.1 (3.3)	1.2 ± 0.1 (3.7)	1.2 ± 0.1 (3.7)
P4	2.5 ± 0.2 (4.6)	1.3 ± 0.1 (2.2)	1.8 ± 0.1 (3.1)	1.8 ± 0.1 (3.1)	3.4 ± 0.1 (6.6)	2.9 ± 0.1 (4.5)
P7	2.7 ± 0.3 (4.2)	3.8 ± 0.1 (7.1)	4.4 ± 0.1 (7)	3.4 ± 0.1 (5.3)	3.8 ± 0.1 (6.9)	3 ± 0.1 (5.3)
P14	4 ± 0.4 (6.5)	4.5 ± 0.1 (6.9)	4.8 ± 0.1 (8.3)	3.5 ± 0.1 (5.7)	4.6 ± 0.2 (8.4)	3.5 ± 0.1 (6.9)
P60	4.6 ± 0.2 (7)	5 ± 0.1 (7.7)	5.2 ± 0.1 (9.2)	4.5 ± 0.1 (7.5)	6.3 ± 0.2 (9.7)	4.4 ± 0.1 (7.5)
P90	4.1 ± 0.2 (6.5)	4.3 ± 0.1 (6.1)	5.2 ± 0.1 (7.9)	5.1 ± 0.1 (7.7)	6.2 ± 0.1 (10.8)	5.1 ± 0.1 (8.1)
P170	3 ± 1 (4.9)	3.9 ± 0.3 (6.6)	3.6 ± 0.2 (6)	3.7 ± 0.4 (5.9)	4.8 ± 0.2 (8.3)	4.4 ± 0.1 (8.1)
P365	4.9 ± 0.5 (6.6)	4.4 ± 0.2 (7.3)	4.3 ± 0.1 (6.2)	3.9 ± 0.2 (4.8)	5 ± 0.3 (9.9)	4.6 ± 0.1 (6.5)

[1]Average length (in micrometers) ± SEM and maximum length noted (in parentheses) of cilia in the cortical layers at different ages. At P0, only upper and deep cortical strata were quantified, and those values were used for layers 2–4 (upper) and layers 5–6 (deep). The same applies to layers 3 and 4 at P4. The subplate at P0 was included in layer 6, but at P4 showed marked differences, with a mean cilia length of 3.8 ± 0.1 lm and a maximum of 5.4 μm.